Journal of Pharmaceutical Analysis 14 (2024) 100901

Contents lists available at ScienceDirect

Journal of Pharmaceutical Analysis

journal homepage: www.elsevier.com/locate/jpa

Original article

YTE-17 inhibits colonic carcinogenesis by resetting antitumor immune response via Wnt5a/JNK mediated metabolic signaling

Hua Sui [a, b, 1], Wanli Deng [c, 1], Qiong Chai [d, 1], Bing Han [e], Yuli Zhang [b], Zhenzhen Wei [a, b], Zan Li [a, b], Ting Wang [f], Jiling Feng [g], Man Yuan [d], Qingfeng Tang [a, **], Hongxi Xu [b, d, *]

[a] Medical Experiment Center, Jiading Branch of Shanghai General Hospital, Shanghai Jiao Tong University School of Medicine, Shanghai, 201803, China
[b] Translational Medicine Research Center for Cancer Prevention and Treatment, Shanghai General Hospital Jiading Branch-School of Pharmacy of Shanghai University of Traditional Chinese Medicine Joint Laboratory, Shanghai, 201803, China
[c] Department of Medical Oncology, Putuo Hospital, Shanghai University of Traditional Chinese Medicine, Shanghai, 200062, China
[d] School of Pharmacy, Shanghai University of Traditional Chinese Medicine, Shanghai, 201203, China
[e] The Second Clinical Medical College of Henan University of Traditional Chinese Medicine, Zhengzhou, 450000, China
[f] Shanghai University of Traditional Chinese Medicine, Shanghai, 201203, China
[g] Precision Research Center for Refractory Diseases, Institute for Clinical Research, Shanghai General Hospital, Shanghai Jiao Tong University School of Medicine, Shanghai, 201620, China

ARTICLE INFO

Article history:
Received 9 May 2023
Received in revised form
11 November 2023
Accepted 16 November 2023
Available online 29 November 2023

Keywords:
Tumor microenvironment
Intestinal epithelial cells
Treg/Th17 cells
Metabolism
Wnt5a/JNK signaling
Tumorigenesis

ABSTRACT

The density and composition of lymphocytes infiltrating colon tumors serve as predictive factors for the clinical outcome of colon cancer. Our previous studies highlighted the potent anti-cancer properties of the principal compounds found in *Garcinia yunnanensis* (YTE-17), attributing these effects to the regulation of multiple signaling pathways. However, knowledge regarding the mechanism and effect of YTE-17 in the prevention of colorectal cancer is limited. In this study, we conducted isobaric tags for relative and absolute quantification (iTRAQ) analysis on intestinal epithelial cells (IECs) exposed YTE-17, both *in vitro* and *in vivo*, revealing a significant inhibition of the Wnt family member 5a (Wnt5a)/c-Jun N-terminal kinase (JNK) signaling pathway. Subsequently, we elucidated the influence and mechanism of YTE-17 on the tumor microenvironment (TME), specifically focusing on macrophage-mediated T helper 17 (Th17) cell induction in a colitis-associated cancer (CAC) model with Wnt5a deletion. Additionally, we performed the single-cell RNA sequencing (scRNA-seq) on the colonic tissue from the Wnt5a-deleted CAC model to characterize the composition, lineage, and functional status of immune mesenchymal cells during different stages of colorectal cancer (CRC) progression. Remarkably, our findings demonstrate a significant reduction in M2 macrophage polarization and Th17 cell phenotype upon treatment with YTE-17, leading to the restoration of regulatory T (Treg)/Th17 cell balance in azoxymethane (AOM)/dextran sodium sulfate (DSS) model. Furthermore, we also confirmed that YTE-17 effectively inhibited the glycolysis of Th17 cells in both direct and indirect co-culture systems with M2 macrophages. Notably, our study shed light on potential mechanisms linking the non-canonical Wnt5a/JNK signaling pathway and well-established canonical β-catenin oncogenic pathway *in vivo*. Specifically, we proposed that Wnt5a/JNK signaling activity in IECs promotes the development of cancer stem cells with β-catenin activity within the TME, involving macrophages and T cells. In summary, our study undergoes the potential of YTE-17 as a preventive strategy against CRC development by addressing the imbalance with the immune microenvironment, thereby mitigating the risk of malignancies.

1. Introduction

Chronic inflammation is a recognized factor contributing to over 20% of cancer cases worldwide [1]. Among these, patients diagnosed with colitis-associated cancer (CAC) often faced advanced-stages diagnoses and poorer prognoses compared to other

* Corresponding author. School of Pharmacy, Shanghai University of Traditional Chinese Medicine, Shanghai, 201203, China.
** Corresponding author.
E-mail addresses: xuhongxi88@gmail.com (H. Xu), tangqingfeng126@126.com (Q. Tang).
[1] These authors contributed equally to this work.

https://doi.org/10.1016/j.jpha.2023.11.008

colorectal cancer (CRC) patients [2]. CRCs originated from intestinal epithelial cells (IECs) of the colon and rectum are impacted by numerous factors including genetics, environment, and chronic, lingering inflammation [3]. Recent studies have highlighted the inflamed microenvironment in promoting genetic mutations within IECs, thereby contributing to tumor development [4,5]. Additionally, the intrinsic connection between IECs and cancer stem cells (CSCs), which possess tumor-initiating capabilities, is crucial for a comprehensive grasp of carcinogenesis.

Previously, our investigations revealed that *Garcinia yunnanensis* (YTE-17) significantly modulates the tumor microenvironment (TME) in azoxymethane (AOM)/dextran sodium sulfate (DSS) mice and $Apc^{Min/+}$ mice with adenomatous polyposis coli (Apc) genetic alterations, offering protective effects against tumor formation [6]. Nevertheless, the precise mechanisms underlying the interplay between IECs and CSCs following YTE-17 exposure, especially within the immunological microenvironment, remain poorly understood. Recent attention has focused on Wnt family member 5a (Wnt5a) as a pivotal regulator orchestrating the response of intestinal stem and progenitor cells to injury, playing a fundamental role in intestinal development [7]. As a ligand predominantly associated with the non-canonical pathway, Wnt5a is most commonly linked to the Wnt5a/planner cell polarity pathway (PCP) signaling cascade. This pathway is well-described in embryogenesis, where it initiates downstream activation of the c-Jun N-terminal kinase (JNK) signaling and the Rho/Rac guanosine triphosphate hydrolases (GTPases), including Rho-kinase (ROCK) [8]. Recent studies have proposed that Wnt5a activates non-canonical Wnt signaling via receptor tyrosine kinase-like orphan receptor (RoR) proteins [9]. Subsequent investigations have affirmed that Wnt5a-receptor tyrosine kinase-like orphan receptor 2 (RoR2) signaling amplifies JNK activation and recruitments of c-Jun to the receptor activator of NF-kappaB (RANK) gene promoter, thereby enhancing the Wnt/JNK pathway-induced signal cascade and activating JNK phosphorylation [10]. However, the precise role of Wnt5a in regulating intestinal immunity and homeostasis remains to be elucidated.

Accumulating evidence underscores the pivotal role of the immune microenvironment in the progression of CSCs, particularly in the context tumor-associated macrophages (TAMs) and various T lymphocytes, notably regulatory T (Treg) cells and T helper 17 (Th17) cells [11]. TAMs have been implicated in promoting tumor progression the secretion of interleukin-10 (IL-10), which increases the frequency of Treg cells, highlighting the potential for reversing the immunosuppressive microenvironment as an effective strategy for CRC therapy [12]. Typically, TAMs exhibit an M2-like phenotype, characterized by an anti-inflammatory and pro-tumor profile [6]. Recent findings, including our own, reveal that M2-like TAMs play a crucial role in reshaping the TME by suppressing the adaptive immune response, especially by controlling TAM polarization and enhancing tumorigenic signaling pathways [13].

In a previous study, we demonstrated that $Apc^{Min/+}$ mice with hereditary polyposis rely on a delicate balance between Treg and Th17 cells in the development of polyps. Furthermore, we observed the presence of a distinct subset of Treg cells exhibiting proinflammatory characteristics [14]. Usually, Treg and Th17 cells are represented as two specific subsets of $CD4^+$ T cells. On the one hand, referred to as suppressor T cells, Treg cells play a crucial role in maintaining self-antigen tolerance, modulating the immune system, and preventing autoimmune disease [15]. On the other hand, Th17 cells, characterized by their expression of the transcription factor ROR-γt and the secretion of IL-17A, are $CD4^+$ T helper lymphocytes influenced by cytokines such as IL-1β, IL-23, and transforming growth factor beta (TGF-β). These cytokines are produced by dendritic cells (DCs) and macrophages, contributing to the induction of Th17 cell differentiation and expansion [16]. Despite the crucial role of ROR-γt^+ Th17 cell expression in sustaining pathologic inflammation in mouse polyposis [17], the specific triggers for its upregulation of ROR-γt in T cells during polyposis and colon cancer remain unclear. Furthermore, it is noteworthy that the *ex vivo* differentiation of Th17 cells coincides with the upregulation of β-catenin and Wnt signaling genes [18], and the deletion of TCF1 promotes the expression of IL-17 by T cells [19]. These observations align with the concept that Wnt/β-catenin signaling actively promotes Th17 cell differentiation.

In this study, we provide evidence that the activation of Wnt5a/JNK signaling constitutes a shared feature within the microenvironment composed of IECs, macrophages, and T cells. Utilizing unbiased isobaric tags for relative and absolute quantification (iTRAQ) analysis on human IECs treated with YTE-17, we have identified Wnt5a/JNK signaling as a key factor in driving intestinal cells toward cancer stem cell phenotype, while also regulating the production and differentiation of both macrophages and T cells. Moreover, we elucidate TME's role in mediating the induction of a cancer stem cell signature by IECs. TAM-mediated Th17 cell differentiation plays an important role in promoting tumorigenesis, which is attenuated following YTE-17 intervention. Intriguingly, alterations in the immune microenvironment enhance β-catenin signaling activity in IECs, facilitating their transformation into CSCs *in vivo*, a phenomenon not observed in response to YTE-17 alone. Our findings suggest that the Wnt5a-JNK-M2 macrophage−β-catenin axis serves as a bridge between environmental factors and the occurrence of CRC by modulating Th17 cell function. This axis may play a significant role in the pathogenesis and development of tumorigenesis disease.

2. Materials and methods

2.1. Cell culture and reagents

Human normal colon epithelial NCM460 cells, murine normal colon epithelial IEC-6 cells, and human monocytic THP-1 cells were procured from the National Collection of Authenticated Cell Cultures (Shanghai, China). NCM460 and IEC-6 cells were cultured in McCoy's 5A and Dulbecco's modified Eagle's medium (DMEM), respectively. THP-1 cells were maintained in THP-1 cell-specific medium (Gibco, Grand Island, NY, USA). All cell lines were supplemented with 10% (*V*/*V*) fetal bovine serum (Gibco) and 1% (*V*/*V*) penicillin/streptomycin (Invitrogen, Carlsbad, CA, USA), and maintained at 37 °C in a humidified incubator with 5% carbon dioxide. Monoclonal antibodies specific for the following proteins were sourced from Abcam (Cambridge, UK) and Cell Signaling Technology (Beverly, MA, USA): Ki67 (# 9449; Cell Signaling Technology, Beverly, MA, USA), proliferating cell nuclear antigen (PCNA) (#13110; Cell Signaling Technology), Wnt5a (ab235966; Abcam), c-Jun (#9165; Cell Signaling Technology), JNK (ab307802; Abcam), p-JNK (#9255; Cell Signaling Technology), protein kinase C-alpha (PKCα) (ab32376; Abcam), ROR2 (ab309483; Abcam), β-catenin (ab32572; Abcam), glyceraldehyde-3-phosphate dehydrogenase (GAPDH) (#5174; Cell Signaling Technology, USA5174S), and β-actin (ab8226; Abcam).

2.2. iTRAQ

In our pursuit of potential diagnostic and prognostic biomarkers to the tumorigenesis process, we executed a quantitative proteomic analysis using the iTRAQ technique on NCM460 cells both in the presence and absence of YTE-17 treatment. The iTRAQ analysis was expertly conducted by Applied Biosystems Incorporation (Carlsbad, CA, USA). Subsequently, the acquired data underwent meticulous

analysis employing the ProteinPilot software, sourced from SCIEX (Framingham, MA, USA) [20]. The total ProtScore, a composite metric that signifies the collective evidential support for a detected protein, was computed by considering all the peptides associated with the respective proteins. Additionally, *P*-values were calculated to gauge the confidence level in discerning discrepancies in average ratios among the various samples.

2.3. Western blot analysis

Cells were lysed in radio immunoprecipitation buffer. Subsequently, protein concentrations in the cell lysate solutions were determined by bicinchoninic acid (BCA) protein assay (Amresco, Solon, OH, USA). Equal amounts of protein were electrophoretically separated by sodium dodecyl sulfate-polyacrylamide gel electrophoresis (SDS-PAGE) in 10% gels and then transferred onto the polyvinylidene difluoride (PVDF) membranes. Following this, the membranes were blocked using 2% (*V*/*V*) bovine serum albumin (BSA) solution in tris buffered saline containing 0.5% (*V*/*V*) Tween 20 TBST buffer for 1 h, prior to incubation of the membranes with primary antibodies against Wnt5a, JNK, p-JNK, ROR2, PKCα, and GAPDH, following well-established procedures [14]. The relative protein levels were determined by calculating the ratio to the level of GAPDH, and the density was quantified using the Quantity One software (v1.8.0).

2.4. AOM/DSS-induced CRC model

The procedures for inducing the CAC model using AOM and DSS were implemented as previously outlined [21]. Mice, aged 5−6 weeks, were subjected to intraperitoneal injection with a single dose of AOM (Merck, Darmstadt, Germany), followed by one-week exposure to 2.5% DSS (MP Biomedicals, Solon, OH, USA) in drinking water. This was succeeded by a two-week recovery period. A total of three DSS cycles of treatment were administered. All experimental protocols and animal welfare considerations were meticulously reviewed and approved by the Animal Ethics Committee of Shanghai University of Traditional Chinese Medicine, China (Approval No.: PZSHUTCM191129007). The housing conditions for the animals strictly adhered to specific pathogen-free standards, in full compliance with the provisions and general recommendations stipulated by Chinese Experimental Animals Administration Legislation.

2.5. Mouse strains and breeding

WNT5A floxed mice ($Wnt5a^{flox/flox}$) mice and Villin-CreER mice were procured from Jackson Laboratory (Bacon, ME, USA). C57BL/6J wild-type (WT) mice were sourced from Shanghai Super B&K Animal Laboratory Co., Ltd. (Shanghai, China), bearing Certification No. SCXK 2016−0018. In summary, the generation of C57BL/6J mice featuring conditional, inducible knockout of *WNT5A* ($Wnt5a^{IEC\text{-}KO}$, tamoxifen) was accomplished by crossing *WNT5A* floxed mice ($Wnt5a^{flox/flox}$) with Villin-CreER mice. As detailed in prior studies [22,23], the WNT5A exon 2 was excised in progeny ($Wnt5a^{IEC\text{-}KO}$ mice) by administering 4-hydroxytamoxifen (HY-16950; Sigma, Darmstadt, Germany) daily to six-week-old mice for a continuous period of seven days. This regimen induced the activation of the Villin-CreER recombinase and facilitated the removal of the floxed WNT5A coding gene. It is worth noting that, as previously confirmed through pharmacokinetic analysis (Fig. S1 and Section S1−S3 in the Supplementary data [6,24]), YTE-17 (25 mg/kg/day) and vehicle group, receiving an equivalent volume (μL) of control oil devoid of YTE-17, were administered orally for a duration of nine weeks, as previously described [6].

2.6. Histology and immunohistochemistry

The entire intestine was promptly extracted upon sacrifice and longitudinally opened after thorough rinsing with ice-cold phosphate-buffered solution (PBS) following established protocols [21]. To determine the incidence of adenoma, the number, location, and size of visible tumors across the intestine were meticulously assessed. Tumor classification involved categorization by size: <3 mm, 3−5 mm, and >5 mm. Subsequently, tissue sections were subjected to fixation in 4% paraformaldehyde in PBS for 10 min at room temperature, succeeded by paraffin embedding. These sections were further subjected to hematoxylin and eosin (H&E) staining for histological evaluation, with assessments conducted by a pathologist who was blinded to the experimental groups. The histopathological analysis encompassed the evaluation of neoplastic lesions and degree of dysplasia, adhering to established criteria and standard classification for colon adenomas.

2.7. Single-cell sequencing

Cell suspensions were loaded onto a Chromium Single Cell instrument (10x Genomics, Pleasanton, CA, USA) to generate single-cell gel beads-in emulsion (GEMs). Subsequently, the single-cell RNA sequence library was prepared employing version 1 of the Chromium Single Cell 3 Library, Gel Bead & Mutiplex Kit (10x Genomics). Sequencing was carried out using Illumina NextSeq500 platform (NovelBio Co., Ltd., Shanghai, China). Prior to downstream analysis, cells were filtered by unique molecular identifier (UMI) number (<100,000 UMIs), gene number (<6000 genes), and mitochondrial gene percentage ('percentage. MT' less than 10%). The analysis utilized Cell Ranger (version 3.0.1) with default parameters, encompassing sample multiplexing, barcode processing, and the quantification of unique molecular indices for single-cell gene expression (https://software.10xgenomics.com/single-cell/overview/welcome).

2.8. Organoid culture

The cultivation of organoids from small intestinal epithelial cells was conducted following previously established protocols [25]. In summary, the resulting organoids were maintained within Matrigel, employing advanced DMEM/F12 medium (HY-K3002; Sigma) that was supplemented with 50 ng/mL epidermal growth factor (EGF) (HY-P70590AF; Sigma), R-Spondin1 conditioned medium (R&D Systems, Minneapolis, MN, USA), and 100 ng/mL Noggin (250-38-1MG; PeproTech, Cranbury, NJ, USA). The cultures underwent a single passage, with crypt length measurements performed under a dissecting microscope. The proliferation of organoid cells was assessed using the Click-iT EdU Imaging System (Invitrogen).

2.9. Cytokine antibody arrays

Serum samples were screened in duplicates using a Mouse Cytokine Array QAM-INF-1 (RayBiotech, Atlanta, GA, USA), which consisted of slides coated with 40 different cytokines. The screening protocol was conducted following the manufacturer's guidelines, with minor adjustments as previously described [14]. In summary, the arrays were initially subjected to a blocking step, followed by an overnight incubation with 100 μL of conditioned medium. Subsequently, biotin-conjugated antibodies (1/250) were applied and incubated for 2 h, followed by an additional incubation with horseradish peroxidase (HRP)-linked secondary antibodies (1/1000) for 1 h. The membranes were incubated with a peroxidase substrate, and the outcomes were documented by the absorbance of the fluorescence. Quantitative analysis of the array data was

conducted utilizing Array Vision Evaluation 8.0 (GE Healthcare Life Science, Marlborough, MA, USA).

2.10. Co-culture system assay

NCM460 cells were co-cultured with M2 macrophages, and it is essential to note that there was no direct cell-to-cell contact in this co-culture system. Briefly, 5×10^3 macrophages were seeded into Transwell inserts (0.4-μm pores; Corning Costar, Corning Inc., Corning, NY, USA), featuring a membrane permeable to liquids but not to cells. NCM460 cells were pre-incubated for 48 h with a YTE-17-conditioned medium, denoted as NCM460 + YTE-17. To assess cell activity within various subgroups of NCM460 cells, the trypan blue method was employed for the cell clonogenic assay. Additionally, for the chemotaxis assay towards cancer stem cells, the capacity of cell lines to form spheres in suspension was evaluated, following established protocols [26]. In order to explore the phenotype of macrophage polarization, macrophages were plated at the bottom of a 24-well plate with different subgroups of NCM460 cells placed in a Transwell chamber. This arrangement ensured that both cell populations were exposed to the same conditions. The characterization of polarization phenotype and activation of signaling pathways in macrophages were assessed through flow cytometry, Western blotting, and quantitative real-time polymerase chain reaction (qRT-PCR), which are described below.

2.11. Formation of colonospheres

To evaluate the capacity of cell lines to form spheres in suspension, a previously described protocol was followed [26]. In Brief, we incubated a limited number of NCM460 cells (100 cells per 200 μL) in serum-free stem cell medium (SCM) to generate primary colonospheres. This medium comprised DMEM/F12 (1:1, *V*/*V*) supplemented with B27 (A1486701; Thermo Fisher Scientific Inc., Waltham, MA, USA), 20 ng/mL EGF (HY-P7067; Sigma), 10 ng/mL fibroblast growth factor (HY-P701238; Sigma), and antibiotic-antimycotic. The incubation was carried out in 24-well ultra low-attachment plates (Corning Inc., Lowell, MA, USA) for 10 days. After the incubation period, the formed colonospheres were centrifuged at 1,000 rpm and dissociated using 0.05% trypsin/ethylenediamine tetraacetic acid (EDTA) and a 22-gauge needle. Subsequently, the dissociated cells were passed through a 40-μM sieve to obtain single-cell suspension. The number and size of the colonospheres formed were assessed under light microscopy (Sigma).

2.12. Flow cytometry

Phenotype analysis of the macrophages and lymphocytes was executed employing a BD FACS AriaII flow cytometer (Becton, Dickinson and Company, Franklin Lakes, NJ, USA), as previously detailed [21]. In brief, the cells were labeled with CD11b-fluorescein isothiocyanate (FITC) (11-0112-82; eBioscience, San Diego, CA, USA), CD206-allophycocyanin (17-2061-82; eBioscience), IL-17-phycoerythrin (PE) (12-7177-81; eBioscience), and F4/80-PE (12-4801-82; eBioscience), according to the manufacturer's recommended protocol. For the assessment of M2 macrophages prevalence, the cells were subjected to incubation with PE-conjugated F4/80 antibodies or allophycocyanin-conjugated CD206. For the analysis of Th17 cell prevalence, the cells were incubated with FITC-conjugated CD4 antibodies or PE-conjugated IL-17 antibodies. Flow cytometry was performed on BD FACSCelesta (BD Biosciences, Franklin Lakes, NJ, USA), and data were analyzed by FlowJo software (FlowJo v10).

2.13. Metabolic analysis by Seahorse

The extracellular acidification rate (ECAR) and oxygen consumption rate (OCR) were assessed using an XF96 Extracellular Flux Analyzer (Agilent, Santa Clara, CA, USA), in accordance with the manufacturer's protocols [27]. Briefly, in the case of ECAR, the glyco-stress test kit (Seahorse Bioscience, Santa Clara, CA, USA) was utilized, which included 10 mM glucose, 50 mM 2-(*N*-(7-nitrobenz-2-oxa-1,3-diazol-4-yl) amino)-2-deoxyglucose, and 2 μM oligomycin. For OCR assessments, the Mito Stress Test Kit (Seahorse Bioscience) was employed, consisting of 1.5 μM fluoro-carbonyl cyanide phenylhydrazone, 2 μM oligomycin, and a pre-mixed solution of 1 μM antimycin A with 100 nM rotenone.

2.14. Immunofluorescence staining

The rehydration and antigen retrieval procedures were performed following the protocols previous described for immunohistochemistry (IHC) staining. Subsequent to blocking with PBS containing 1% (*V*/*V*) BSA and 0.3% (*V*/*V*) Triton, sections were subjected to overnight incubation at 4 °C with primary antibodies targeting Wnt5a and JNK. On the subsequent day, fluorescently labeled secondary antibody and 4',6-diamino-2-phenylindole (DAPI) were applied for a duration of 1 h. The slides were scanned using the tile scan function of the Leica confocal microscope TCS SP8 (Wetzlar, Germany). For IHC tumors in AOM/DSS model, tissue sections were incubated overnight with a primary antibody against β-catenin at 4 °C. Following the primary antibody, sections were further incubated with a secondary antibody. Staining percentages were analyzed using ImageJ software.

2.15. qRT-PCR

Total RNA was extracted from CRC cells and tumor tissues using the eRNeasy Mini Kit (Takara Bio, Dalian, China). Subsequently, 1 μg of total RNA was reverse transcribed to assess relative messenger RNA (mRNA) expression with PrimeScript™ RT reagent Kit (Takara Bio Inc., Beijing, China). Target complementary DNAs (cDNAs) were then amplified and quantified using SYBR Green (Takara Bio Inc.) on a QuantStudio Flex 7 Real Time PCR system (Quantstudio Real Time PCR software v1.7.2; Applied Biosystems Incorporation). All reactions were performed in triplicate and normalized to GAPDH by $2^{-\Delta\Delta C_T}$ method. Validated qRT-PCR (mouse/human specific) primers for Gata3, T-bet, tumor necrosis factor-alpha(TNF-α), forkhead box protein 3 (FOXP3), RoR-γt, IL-17, IL-21, IL-22, interferon-alpha (IFN-α), IL-12, IL-10, and GAPDH were obtained from SA Biosciences (Qiagen, Dusseldorf, Germany). The Primer sequences are provided in Table S1.

2.16. Statistical analysis

Three biological replicates were performed and all numerical data are presented as means ± standard deviation (SD) or means ± standard error of mean (SEM). Statistical analyses were conducted using Prism 8.0 (GraphPad Software, Inc.) and SPSS 23.0 (IBM, Chicago, IL, USA). Differences between two groups were compared with Mann-Whitney *U* test or Student's *t*-test. Differences among multiple groups were assessed using one-way analysis of variance (ANOVA) followed by Duncan's test. These statistical methods were applied for the analyses of various parameters, including colon tumor numbers, IHC, Western blot, enzyme-linked immunosorbent assay (ELISA), cell viability, qRT-PCR, and transwell migration assays. For the analysis of gut microbiome in mice, the Wilcoxon rank-sum test was utilized. The results are based on data from a minimum of three independent

experiments. Significance levels were denoted as follows: $^{*}P < 0.05$ and $^{**}P < 0.01$; $^{\#}P < 0.05$ and $^{\#\#}P < 0.01$.

3. Results

3.1. YTE-17 suppresses intestinal tumorigenesis and is associated with Wnt5a signaling

Garcinia yunnanensis, a local food in Cangyuan, Yunnan, China, has demonstrated promising anti-tumor properties in the context of inflammatory CRCs development [6]. Previous reports have identified oblongifolin C (OC) and guttiferone K (GUTK) as the primary active components of *Garcinia yunnanensis*, constituting over 80% of its composition in a ratio of 1:1 (Figs. 1A, S1A, and S1B). In order to quantitatively investigate the controllable and safe concentration levels of YTE-17 *in vivo*, the main pharmacokinetic results based on the non-compartment model analysis are summarized in Fig. S1C. Therefore, this study focused on investigating the combined effects and preventive mechanisms of these two components, referred to as YTE-17, utilizing a purification technique. Consistent with prior findings that established non-toxic doses in RAW264.7 cells and CRC cells [6], the doses of YTE-17 ranging from 0 to 2 μM had minimal impact on the cell viability of IECs (Fig. 1B).

To delve deeper into the mechanistic targets of YTE-17 in the context of CRC prevention, iTRAQ analysis was performed to analyze differential protein expression in NCM460 cells treated with varying concentrations of YTE-17, as depicted in Fig. 1C. Importantly, our analysis revealed a reduction in the protein expression of key components of Wnt5a/PCP signaling pathway in NCM460 cells after YTE-17 treatment, including WNT5, JUN, and ROR2. Subsequently, Western blot analysis was employed to assess the expression of Wnt5a signaling pathway-related proteins in NCM460 cells treated with YTE-17 for 24, 48, and 72 h. Consistently, we observed a substantial decreased in the protein expression of Wnt5a, JNK, p-JNK, and ROR2 in a time and dose-dependent manner compared to control conditions (Figs. 1D and E).

Given that Wnt5a a pivotal factor in malignancy of epithelial cells following YTE-17 treatment *in vitro*, we proceeded to employ *Wnt5a*$^{IEC\text{-}KO}$ mice to investigate the role of YTE-17 in AOM/DSS-induced CRC. The structural details of the established model are presented in Fig. 1F. As numerous reports have indicated that conditional knockout of host Wnt5a significantly reduces tumor formation and metastatic tumor burden [28,29], we subsequently explored the immunosuppressive microenvironment effects of Wnt5a during the growth and development of intestinal epithelium in mice. In line with other previous studies, there were no observable morphological changes in the intestines or changes in animal survival, even weeks or several months after Wnt5a deletion (Figs. 1G and S2A and Section S4 in the Supplementary data [6,30,31]). Western blot analysis confirmed near-complete loss of Wnt5a in intestinal epithelial tissue from Wnt5a$^{IEC\text{-}KO}$ animals (Fig. 1H), underscoring the high efficiency of the knockout.

Subsequently, the mice were subjected to the treatment regimen outlined in Fig. 1I, and we monitored changes in disease activity index (DAI) as illustrated in Fig. S2B and Section S5 in the Supplementary data [32,33]. As anticipated, in comparison to the AOM/DSS controls group, the proliferation rate within colon adenocarcinoma of AOM/DSS mice was notably affected by the loss of Wnt5a (Figs. 1J and S2C and Section S5 in the Supplementary data [34,35]). Following the AOM/DSS treatment, a significant decline in body weight was observed (Fig. 1K), along with a reduced incidence of colon adenomas (Fig. 1L) and a decrease in tumor (Figs. 1L and S2D) in *Wnt5a*$^{IEC\text{-}KO}$ mice. These findings collectively suggest that the absence of Wnt5a is effective in protecting against AOM/DSS-induced colitis-associated tumorigenesis.

3.2. Intestinal stem cells contribute Wnt5a signaling to the CRC TME

As Ki67 and PCNA serve as cell proliferation markers, we conducted IHC to assess their localization and expression levels, along with the expression of Wnt5a signaling pathway-related genes (including Wnt5a, JNK, and PKCα) in the tumors from *Wnt5a*$^{IEC\text{-}KO}$ mice following AOM/DSS treatment. Similar to prior reports, we observed mild alterations in glandular structure coincident with chief cell loss in *Wnt5a*$^{IEC\text{-}KO}$ mice after AOM/DSS treatment compared to WT mice following the same treatment (Figs. 2A and S3A). Histologically, the lesionsin *Wnt5a*$^{IEC\text{-}KO}$ mice after AOM/DSS treatment exhibited more adenocarcinomas with lower grade, frequently invading the submucosa and muscularis propria compared to those in WT mice after AOM/DSS treatment (Fig. 2A).

A substantial body of evidence suggests that Wnt5a plays a role in maintaining a stem cell-like expression pattern in tumor cells [8,30]. Therefore, we generated tumor organoids using single cells derived from adenomas of *Wnt5a*$^{IEC\text{-}KO}$ mice after AOM/DSS treatment. Organoid culture of the WT mouse-derived intestinal epithelial cells revealed budding from cysts, forming mini-crypt structures (Fig. 2B), consistent with previous reports [36]. We further assessed the size of individual organoids (Figs. 2B and C, up) and evaluated the epithelial cell proliferation in the organoids by quantifying the number of organoids (Figs. 2B and C, down). Western blot results also demonstrated that the expression of several Wnt5a target genes and intestinal stem cell-specific markers Lgr5^{+} were reduced in colon tissues of *Wnt5a*$^{IEC\text{-}KO}$ mice after AOM/DSS treatment (Fig. 2D).

To identify significant changes in inflammatory cytokines, we employed a cytokine antibody array to illustrate the supernatant of colonic tissue (Fig. 2E (left) and S3B). Compared to WT mice, *Wnt5a*$^{IEC\text{-}KO}$ mice after AOM/DSS treatment secreted higher levels of inflammatory cytokines/chemokines including IL-17, IL-4, TNF-α, T-cell activation-3 (TCA-3), Fas ligand (FasL), and macrophage inflammatory protein-1γ (MIP-1γ) (Fig. 2E, middle). Notably, predictions of gene phenotypes indicated a strong association with macrophage and T lymphocytes differentiation based on Gene Ontology (GO) pathway methodology analysis (Fig. 2E, right). Additionally, we observed downregulated mRNA expression of T-helper cells-related targets and inflammatory cytokines/chemokines in colon tissues of *Wnt5a*$^{IEC\text{-}KO}$ mice after AOM/DSS treatment compared to those in WT mice after AOM/DSS treatment (Fig. 2F). These findings suggest that the antitumor effect of YTE-17 mediated Wnt5a appears to be attributed to its modulation of T-cell immunity.

3.3. Single-cell RNA sequencing (scRNA-seq) reveals heterogeneity for TAMs in the TME

To delineate various immune cell subsets associated with tumor growth, we conducted scRNA-seq analysis on local tumor cells from colon tissues of normal and *Wnt5a*$^{IEC\text{-}KO}$ mice under the AOM plus DSS mouse CRC model. The results revealed nine immune cell clusters, with higher cell counts observed among epithelial cells, mononuclear granulocytes, and T cells (Fig. 3A). Notably, the hallmark gene set for M2 macrophages was more enriched in *Wnt5a*$^{IEC\text{-}KO}$ mice sample compared to normal samples (Fig. 3B). These

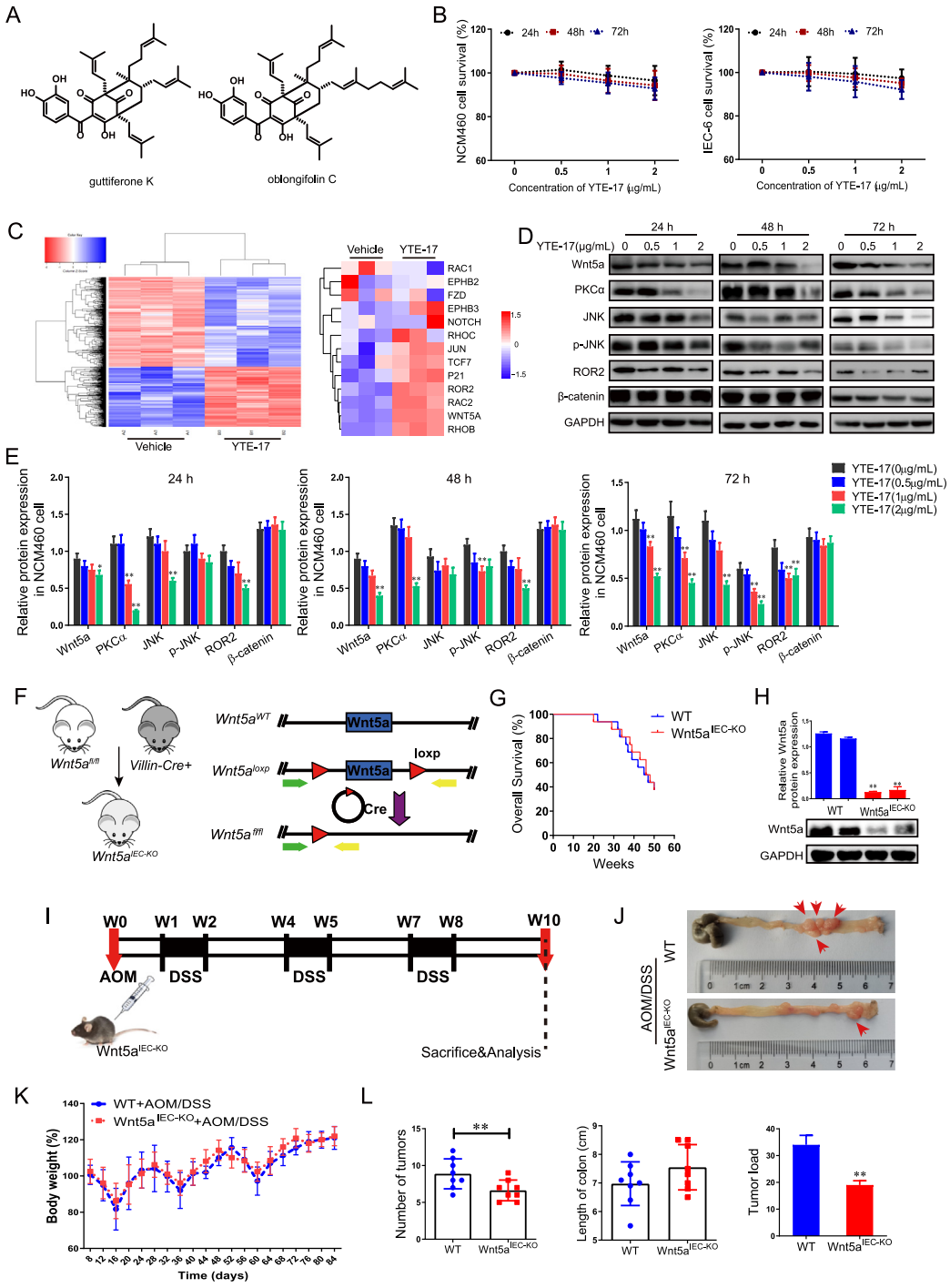

Fig. 1. *Garcinia yunnanensis* (YTE-17) prevent tumorigenesis effect is Wnt family member 5a (Wnt5a) dependent. (A) Structure of oblongifolin C (OC) and guttiferone K (GUTK). (B) Proliferation of NCM460 and IEC-6 cells were assayed respectively at 24-, 48- and 72-h post-treatment with YTE-17 (OC and GUTK). Cells were treated with YTE-17 at 0.5, 1, and 2 μg/mL respectively. Data indicate means ± standard deviation (SD) of three separate experiments as triplicates. (C) Isobaric tags for relative and absolute quantification (iTRAQ) analysis of differential protein expression in NCM460 cells with or without YTE-17 treatment (a heat map of highly variable proteins detected in iTRAQ analysis in NCM460 cell with or without YTE-17 treatment ($n = 3$ each) (left) and differentially enriched proteins in Wnt5a pathway identified by expression analysis (right)). (D, E) Western blots showing expression levels of Wnt5a, protein kinase C-alpha (PKCα), c-Jun N-terminal kinase (JNK), *p*-JNK, receptor tyrosine kinase-like orphan receptor 2 (ROR2) and β-catenin in NCM460 cells after YTE-17 treatment for 24, 48, and 72 h: representative Western blot images (D) and relative density analysis (E) of different proteins, with glyceraldehyde-3-phosphate dehydrogenase (GAPDH) as the loading control. Representative data from three experiments are shown as mean ± SD. $^{*}P < 0.05$ and $^{**}P < 0.01$ vs. YTE-17 at 0 μg/mL, by two-way one-way analysis of variance (ANOVA) (means ± SD). (F) Schematic of experimental design on inducible knockout of *WNT5A* (*Wnt5a*$^{IEC\text{-}KO}$) mice. (G) Survival rate analysis of *Wnt5a*$^{IEC\text{-}KO}$ mice and wild-type (WT) mice ($n = 16$/group). (H) Western blotting analysis on the difference of Wnt5a expressions between the adenomas of *Wnt5a*$^{IEC\text{-}KO}$ mice and that of the WT mice. $^{**}P < 0.01$ vs. WT mice. (I) Schematic illustration of azoxymethane (AOM)/dextran sodium sulfate (DSS)-induced colitis−associated colorectal cancer (CRC) model. (J–L) Effects of Wnt5a deficiency on the microscopic view of the colon tumor (J), body weight (K), and number of intestinal polyps and colon length (L) in WT and *Wnt5a*$^{IEC\text{-}KO}$ mice treatment with AOM/DSS. Data are given as means ± SD of eight animals in each experimental group, with Welch's correction, one-tailed *t*-test. $^{**}P < 0.01$ vs. WT mice treatment with AOM/DSS. *Wnt5a*$^{flox/flox}$: *WNT5A* floxed mice; IEC: intestinal epithelial cells; Cre: cyclization recombinase.

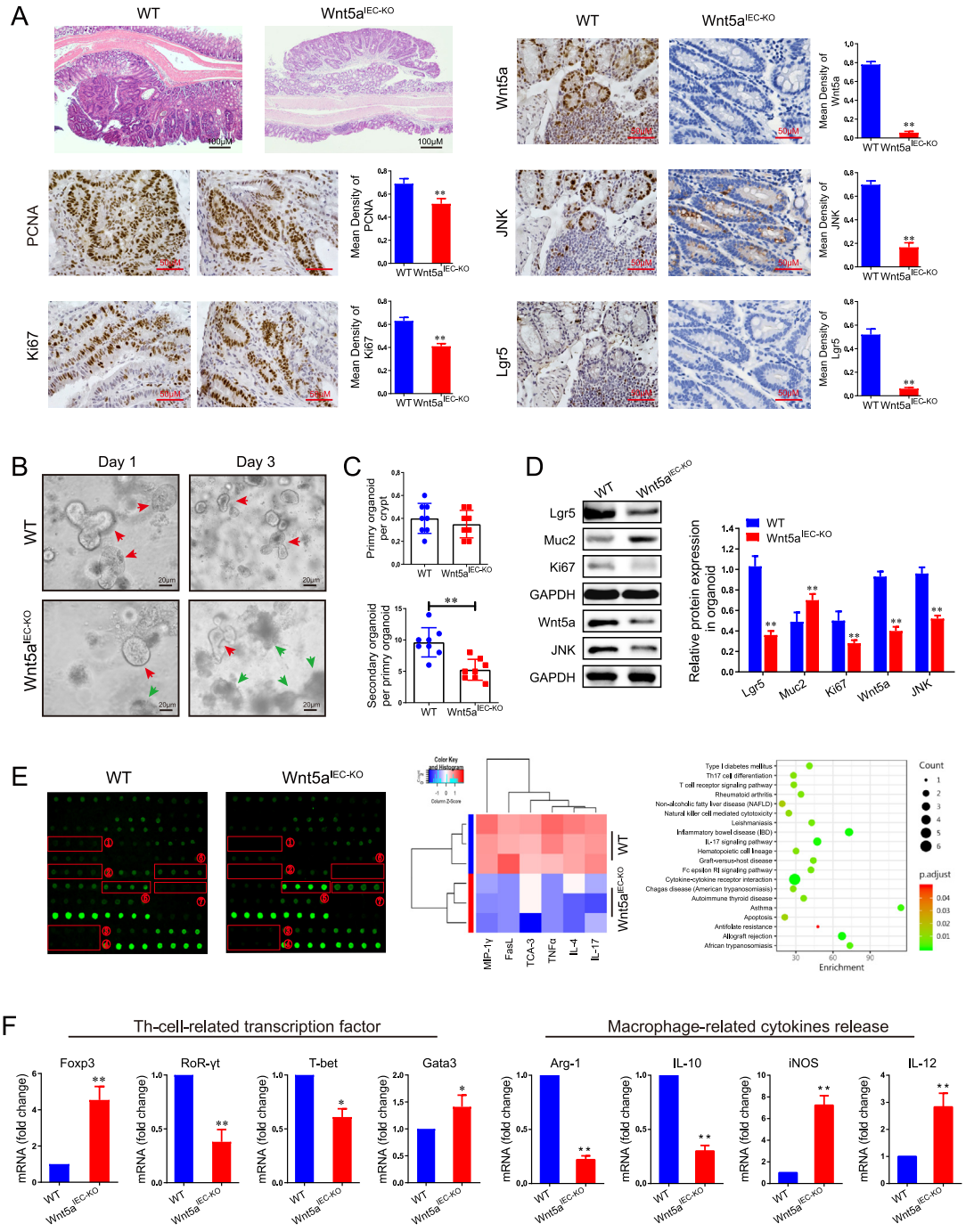

Fig. 2. Wnt family member 5a (Wnt5a) deficiency attenuated the capabilities of these cancer stem cells (CSCs) in tumor initiation and phenotype of T helper cells in colorectal cancer (CRC) mice model. (A) Effects of Wnt5a deficiency on tumor histology and the expression of proliferating cell nuclear antigen (PCNA), Ki67, Wnt5a, c-Jun N-terminal kinase (JNK), and Lgr5 in CRC mice (n = 8/group). (B) Representative pictures of tumor organoids derived from small intestinal epithelial cells obtained from in wild-type (WT) and inducible knockout of *WNT5A* (*Wnt5a*$^{IEC\text{-}KO}$) mice. After isolation, organoids were kept in epidermal growth factor (EGF), Noggin, and RSPO1 (ENR media). Pictures were taken seven days after passaging in case of passages 1 and 3. (C) Effects of Wnt5a deficiency on primary organoid per crypt (up) and secondary organoid per primary organoid (down) in WT and *Wnt5a*$^{IEC\text{-}KO}$ mice induced by azoxymethane (AOM)/dextran sodium sulfate (DSS). (D) Representative Western blot images of different proteins in organoid of WT and *Wnt5a*$^{IEC\text{-}KO}$ group. (E) Effects of Wnt5a deficiency on inflammatory cytokines *in vitro*. Proteins obtained from the intestinal tumor in WT and *Wnt5a*$^{IEC\text{-}KO}$ mice was analyzed using the murine proteome profiler cytokine array according to the manufacturer's specifications. Any spots exhibiting differential expression were marked with a box (left). The discrepancy in inflammatory cytokines between the two groups was evaluated utilizing a cytokine antibody array (middle). Fisher's exact test was used to analyze categorical data through clusterProfiler from R/Bioconductor (right). The selected criterion is the number of proteins that fall on a term/Gene Ontology (GO) ≥ 2 and P value < 0.05. Drawing the term/GO is in descending order of size according to the count value. (F) Messenger (mRNA) expressions of T helper cell related transcription factor including forkhead box protein 3 (Foxp3), receptor tyrosine kinase-like orphan receptor-gamma t (ROR-γt), T-bet, Gata3, and T helper cell cytokines including interleukin-22 (IL-22), IL-17, and IL-21 in intestinal epithelial cells (IECs) were detected by quantitative real-time polymerase chain reaction (qRT-PCR). The data are presented as the mean ± standard deviation (SD) (n = 5), with Welch's correction through one-tailed t-test. $^{*}P < 0.05$ and $^{**}P < 0.01$ vs. WT mice treatment with AOM/DSS administration. GAPDH: glyceraldehyde-3-phosphate dehydrogenase; MIP-1γ: macrophage inflammatory protein-1γ; FasL: Fas ligand; TCA-3: T-cell activation-3; TNF-α: tumor necrosis factor-alpha. iNOS: inducible nitric oxide synthase; RI: receptor IgE.

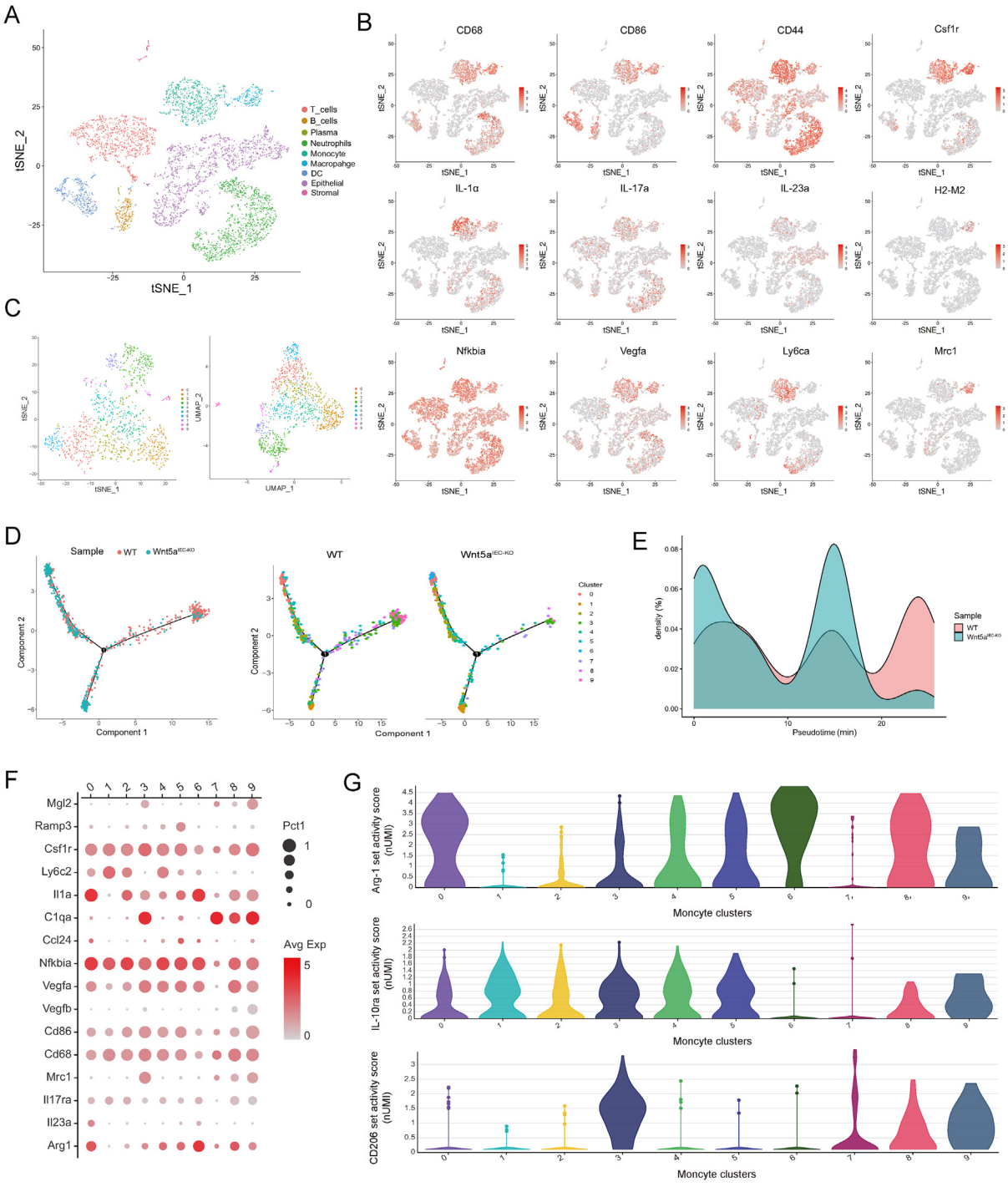

Fig. 3. Single-cell profiling of colonic immune cells between normal and Wnt family member 5a (Wnt5a) deficiency colorectal cancer (CRC) mice model. (A) Intestinal tumor tissue from wild-type (WT) and inducible knockout of *WNT5A* (*Wnt5a*$^{IEC\text{-}KO}$) CRC mice were processed into single-cell suspension and unsorted cells were used for single-cell RNA sequencing (scRNA-seq) with 10x Genomics. (B) Expression levels of selected known hallmark genes among various types of immune cells (T cells, B cells, plasma, neutrophils, monocyte, macropahge, dendritic cells (DCs), epithelial, and stromal cells). (C) *t*-distributed stochastic neighbor embedding (*t*-SNE) and uniform manifold approximation and projection (UMAP) showing the composition of macrophagels (TAMs) colored by cluster. Red dashed circle shows M2 macrophages with nine clusters in each plot. Each cluster was displayed in a unique color. 0: Mono_Il1a^{+}; 1: Mono_Ly6c2^{+}Cd86^{+}; 2: Mono_ Ly6c2^{+}Cd86^{+}; 3: Mono_Csf1r^{+}; 4: Mono_Ly6c2^{+} Cd44^{+}; 5: Mono_Ramp3^{+}; 6: Mono_IL17ra^{+}; 7: Macro_F4/80^{+}; 8: Macro_CD11b^{+}; and 9: Macro_F4/80^{+}CD206^{+}. (D)Cancer stem cells (CSCs) from WT and *Wnt5a*$^{IEC\text{-}KO}$ mice induced by azoxymethane (AOM)/dextran sodium sulfate (DSS) samples ordered along pseudotime trajectories, colour-coded by clusters. Trajectory of macrophages along pseudotime in a two-dimensional space. Each point corresponds to a single cell. Cluster 0: Mono_Il1a^{+}; Cluster 1: Mono_Ly6c2^{+}Cd86^{+}; Cluster 2: Mono_ Ly6c2^{+}Cd86^{+}; Cluster 3: Mono_Csf1r^{+}; Cluster 4: Mono_Ly6c2^{+}Cd44^{+}; Cluster 5: Mono_Ramp3^{+}; Cluster 6: Mono_IL17ra^{+}; Cluster 7: Macro_F4/80^{+}; Cluster 8: Macro_CD11b^{+}; and Cluster 9: Macro_F4/80^{+}CD206^{+}. (E) Density illustrating the dynamic changes of gene expression along pseudotime. The differentially expressed genes (DEGs) were clustered hierarchically into two groups, and the representative enriched pathways of each group were shown. (F) Bubble plot illustrating gene expression patterns of M2-macrophage cells. The dot size represents the proportion of expressing cells, which are colored according to *Z* score-normalized expression. (G) Violin plots illustrating gene expression patterns among distinct subpopulations of macrophage cells. The *y* axis shows the log scale-normalized read counts. The ten single-cell clusters were associated with various gene signatures, and the relative overrepresentation of a gene signature for a given cluster was calculated using the one-tailed Mann-Whitney test. IL: interleukin; IEC: intestinal epithelial cells.

characteristics likely reflect interactions among stromal cell during tumor initiation, linking macrophages, T cells, and intestinal epithelial cells to remodel the CRC microenvironment (Fig. 3C). Pseudo-time analysis indicated that TAMs originated from macrophages and tended to differentiate toward M2 macrophages (Figs. 3D and E). Among all the macrophage subclusters, the gene expression profile of Arg-1 and CD206 was highly expressed in *Wnt5a*$^{IEC\text{-}KO}$ mouse samples (Figs. 3F and G), suggesting that TAMs represent a transitional stage mononuclear granulocytes that has recently migrated to the TME and are undergoing conversion from M1 macrophages to M2 macrophages. Similar findings have been reported by others, highlighting the transition of macrophage populations from pro-inflammatory macrophages to immune-suppressive subsets in normal tissue through dysplasia to cancer, as revealed by scRNA-Seq [37]. Additionally, scRNA-Seq analysis of murine tumor granulocytic myeloid-derived suppressor cells (G-MDSCs) has highlighted a unique ApoE G-MDSC subset enriched with TAM blockade [38].

3.4. YTE-17 -induced antitumor T-cell immunity is macrophage dependent

As we previously demonstrated, YTE-17 inhibits the polarization of M2 macrophages during CRC procession [6]. Neverthless, the interaction between macrophages and IECs remained unclear. To investigate whether the presence of YTE-17 affects TME effects *in vitro*, we co-incubated IECs with M2 macrophages isolated from the bone marrow-derived macrophages (BMDMs) of AOM/DSS mice (Fig. 4A). Prior to the co-culture, BMDMs were stimulated with IL-4 for M2 macrophage polarization, and IECs were treated with YTE-17 for 48 h (Fig. S4A). As anticipated, M2 macrophages increased the proliferation of IECs, while this effect was significantly mitigated by YTE-17 treatment of IECs cells (Figs. 4B and S4B).

Cell growth, a fundamental step in tumorigenesis progression, can be analyzed through sphere-forming assays. In our study, we used stem cell medium to assess sphere-forming capacity (Fig. 4C). The sphere numbers (Fig. S4C) and the size of the spheres (Fig. 4C), as evaluated by cell number per sphere, were significantly increased in NCM460 coculture with M2 macrophage compared to control IECs. Notably, YTE-17 almost completely halted M2 macrophage-mediated proliferation of NCM460 cells, indicating that YTE-17 intervention in NCM460 cell lines also inhibited macrophage-induced stem differentiation of intestinal cells (Fig. 4C). Moreover, M2 macrophage appeared to increase Wnt5a and JNK expression, which was attenuated by YTE-17 interference, as evidenced by Immunofluorescence analysis in IEC spheres (Fig. 4D).

To investigate the mechanism of macrophages action on intestinal epithelial cells, we co-cultured NCM460 cells with M2 macrophages in a Transwell system, with IECs in the upper chamber and macrophages in the lower chamber (Fig. 4E). Co-cultured IECs significantly increased the expression of CD206 and decreased the expression of the M1 markers CD11b in both BMDMs and THP-1 cells. These effects were attenuated by YTE-17 intervention, suggesting that YTE-17-affected IECs contribute to reversing M2 macrophage polarization (Fig. 4F). Flow cytometric analysis yielded similar results. YTE-17-affected IECs significantly restrained the expression of the M2 marker (Arg-1) and JNK pathway-related proteins in BMDMs and THP-1 cells, which were induced to become M2 macrophages (Fig. 4G). Consistent with the qRT-PCR data, ELISA results showed that the expression of IL-1β, IL-6, IL-10, and TGF-β in co-culture system was significantly decreased by the presence of BMDMs, whilst IL-12 and TNF-α were elevated. All these effects were attenuated by YTE-17 intervention, as shown in Fig. 4H.

3.5. Wnt5a-activated M2 macrophage reprograms YTE-17 metabolic mode

Next, we studied the mechanisms underlying the YTE-17-mediated antitumor T-cell immunity dependent on M2 macrophage (Fig. 5A). *In vitro*, we stimulated purified $CD4^{+}CD25^{-}$ T cells with TGF-β combined with IL-6 or IL-2 in the presence or absence of M2 macrophage. We observed a significant increase in the frequency of $IL\text{-}17^{+}$ T cells in co-culture system after exposure to IECs-affected M2 macrophage (Fig. 5B). Specifically, M2 macrophage-induced IL-17 production was significantly decreased in the YTE-17-affected NCM460 cell co-cultured with M2 macrophage group compared to the co-culture control group (Fig. 5B). We then examined the effect of YTE-17 on the mRNA expression of IL-17, ROR-γt, IL-10, and IL-12, which are considered as the master regulators of Th17 cell and M2 macrophage development and function in the immune system of mice. Notably, consistent with the regulation of Treg/Th17 cell balance and M2 macrophage polarization in coculture system, the ELISA analysis revealed a significant increase in the production of IL-17 and IL-10 and a significant decrease in the production of ROR-γt and IL-12 in the co-culture system, compared with that in no-treatment macrophage co-culture system (Fig. 5C).

In addition, macrophage polarization not only causes phenotypical alterations in Th17 cell but also reprogrammed their metabolic mode. Based on an analysis of scRNA-seq data obtained from CRC patients in a previously published study [39], we observed a prominent group of gene related to glycolytic metabolisms that were differentially expressed in different Th17 cell phenotypes (Fig. 5D, left). Additional gene set enrichment analyses confirmed the specific enrichment of the glycolytic pathway in colonic intratumoral Th17 cells (Fig. 5D, right). Moreover, we found that Th17 cells treated with IECs-conditioned macrophage exhibited a decreased in OCR, indicating a shift towards mitochondrial oxidative respiration, and an increase in ECAR reflecting overall glycolytic flux (Fig. 5E). Additionally, we confirmed that macrophage stimulation significantly upregulated the activity of the glycolytic pathway in Th17 cells, as evidenced by increased glucose uptake, pyruvate level, adenosine triphosphate (ATP) level, and lactate production in Th17 cell (Fig. 5F).

To investigate the mechanism of Th17 cell on M2 macrophages, we used an indirect co-culture system as a Transwell configuration, in which the M2 macrophage were placed in the upper chamber, and the Th17 cells were located in the lower chamber (Fig. 5G). Consistent with previous findings, M2 macrophage promoted the differentiation and activity of Th17 cells, which was attenuated by YTE-17 intervention (Figs. 5H-J, and S5). Furthermore, in line with the glycolysis results from the co-culture systems, the effects of indirect co-culture systems on Th17 cells were also enhanced by IECs-conditioned macrophage, suggesting that YTE-17 profoundly regulates the metabolic mode of Th17 cells via an IECs-M2 macrophage pathway, inhibiting their antitumor effect.

3.6. Th17 cell is essential for Wnt5a-mediated tumorigenesis via M2-like macrophages

To confirm the function of Th17 cells in increased tumor load observed in *Wnt5a*$^{IEC\text{-}KO}$ mice, we treated mono-housed WT and *Wnt5a*$^{IEC\text{-}KO}$ mice with anti-Th17 antibody during the AOM-DSS

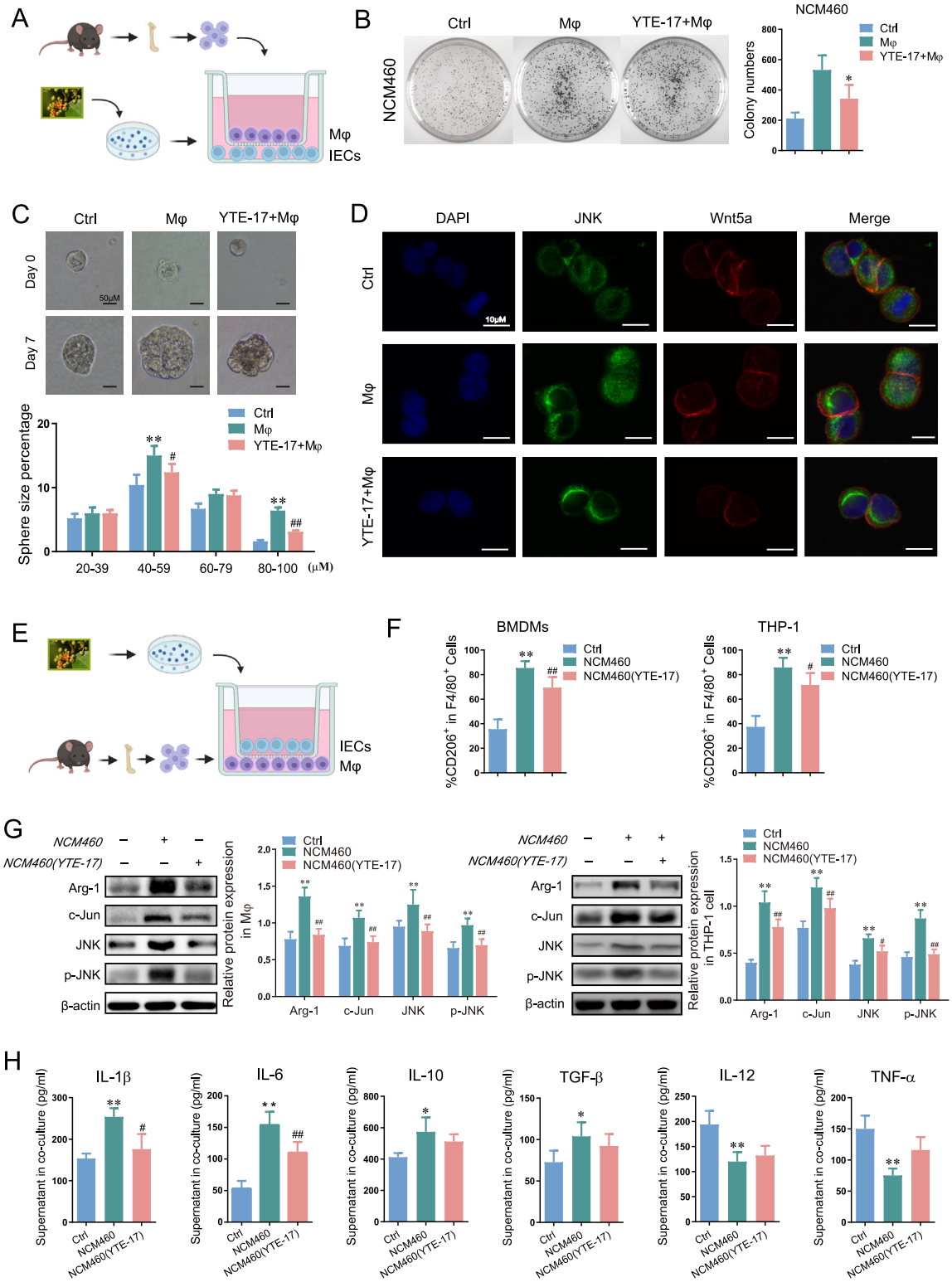

Fig. 4. *Garcinia yunnanensis* (YTE-17) inhibited M2 macrophage polarization through regulating intestinal epithelial cells (IECs). (A) Schematic representation of co-culture with macrophage and intestinal epithelial cells (IECs) in Transwell chamber. (B) After incubation with YTE-17 (2 μg/mL) for 48 h, the IECs were co-cultured with bone marrow-derived macrophages (BMDMs) (macrophage in image), which were at the Transwell inserts. IECs include human NCM460 cell and mice IEC-6 cell. Macrophages include human THP-1 cell and mice BMDMs. IECs were located at the bottom of the cell plate, the number of living IECs cells was measured by clone formation assay. (C) NCM460 cells were cultivated *in vitro* sphere-forming assays using various treatments: phase contrast photos (up) and the average of sphere numbers from three independent experiments (down). (D) Immunofluorescence micrographs of catenin (green) and 4′,6-diamidino-2-phenylindole (DAPI) (blue) expressions in different group NCM460 cells. (E) Interchangeable positions of macrophages and intestinal epithelial cells in Transwell chamber follow withFig. 4A. (F) M2 macrophages were analyzed by using a flow cytometry analysis of $CD206^{+}$, $F4/80^{+}$ cell fraction in BMDMs and THP-1 cells as shown in Fig. 4E. (G) Western blot analysis of Arg-1, c-Jun, c-Jun N-terminal kinase (JNK), and the phosphorylation of JNK expression in BMDMs and THP-1 cells after coculture with different group NCM460 cells. (H) Interleukin-1β (IL-1β), IL-6, IL-10, transforming growth factor beta (TGF-β), IL-12, and tumor necrosis factor-alpha (TNF-α) levels in coculture supernatant were evaluated using enzyme-linked immunosorbent assay (ELISA) analysis. The data are presented as the mean ± standard deviation (SD) ($n = 3$), with Welch's correction, two-tailed *t*-test. $^{*}P < 0.05$ and $^{**}P < 0.01$ vs. control; $^{\#}P < 0.05$ and $^{\#\#}P < 0.01$ vs. NCM460. *Wnt5a*: Wnt family member 5a.

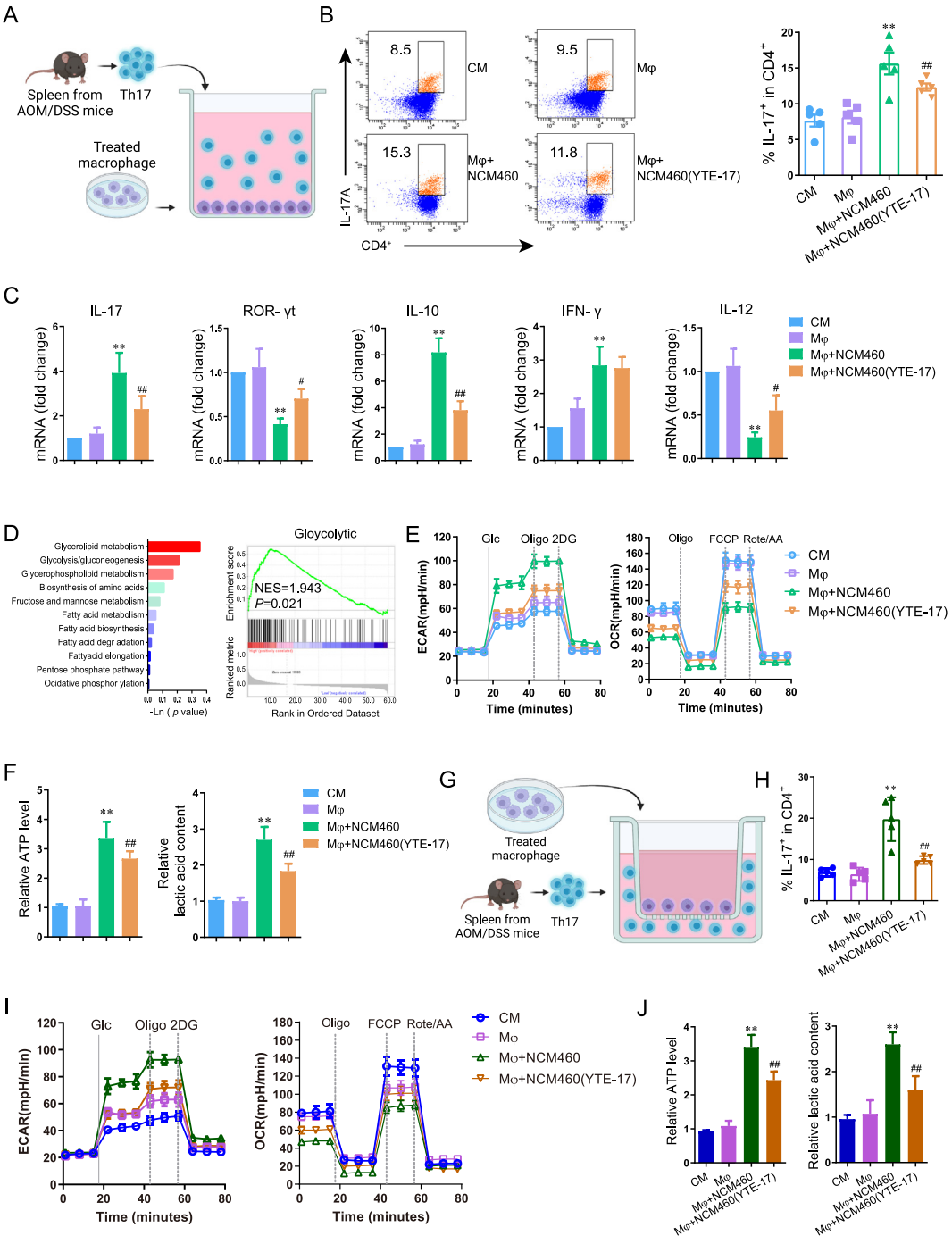

Fig. 5. *Garcinia yunnanensis* (YTE-17) regulated metabolic reprogramming through regulating M2 macrophage mediated T helper 17 (Th17) cell. (A) Schematic representation of M2 macrophage were cocultured with Th17 cells. (B) After incubation with intestinal epithelial cells (IECs) (1:1 ratio) as described in Fig. 4A, M2 macrophage were co-cultured with Th17 cells, which were at the bottom of six-well plate. Th17 cells were suspended in co-culture medium, the phenotype of Th17 cells was measured by a flow cytometry analysis. (C) Messenger RNA (mRNA) expressions of Th17 cell cytokines including interleukin-12 (IL-12), IL-17, IL-10, and receptor tyrosine kinase-like orphan receptor γt (ROR-γt) in Th17 cells were detected by quantitative real-time polymerase chain reaction (qPCR). (D) Different expression of glycolytic metabolisms in colorectal cancer (CRC) patients and gene set enrichment analysis (GSEA) assay with different Th17 cell phenotypes. Differently expressed genes (DEGs) between various Th17 cell from patients with CRC (GSE108989) were analyzed for metabolic pathway enrichment (left). Significantly different pathways ($P < 0.01$) are highlighted in red. Glycolysis-related genes were significantly enriched in DEGs between colonic intratumoral and Th17 cell, according to GSEA (right). (E) Extracellular acidification rate (ECAR) (left) and oxygen consumption rate (OCR) (right) in Th17 cell were measured with or without macrophage direct contact co-culture. (F) Adenosine triphosphate (ATP) level were detected by ATP Luminescent Cell Viability Assay Kit: ATP level in the co-culture supernatants (left) and lactate secretion in the co-culture supernatants detected by L-lactate assay (right). (G) After incubation with IECs (1:1 ratio) as described in Fig. 4A, M2 macrophage were indirect co-cultured with Th17 cells, which were at the Transwell inserts. (H) Th17 cells were suspended in co-culture medium and the phenotype of Th17 cells from indirect co-culture system was measured by a flow cytometry analysis. (I) ECAR (left) and OCR (right) in Th17 cell were measured with or without macrophage indirect contact co-culture ($n = 3$). (J) ATP level were detected by ATP Luminescent Cell Viability Assay Kit: ATP level in the indirect contact co-culture supernatants (left) and lactate secretion in the indirect contact co-culture supernatants detected by L-lactate assay (right). The data are presented as the mean ± standard deviation (SD) ($n = 3$), with Welch's correction, two-tailed *t*-test. $^{*}P < 0.05$ and $^{**}P < 0.01$ vs. macrophage; $^{\#}P < 0.05$ and $^{\#\#}P < 0.01$ vs. macrophage + NCM460. AOM: azoxymethane; DSS: dextran sodium sulfate; CM: culture medium; IFN-α: interferon-alpha; 2DG: 2-deoxy-D-glucose; FCCP: carbonyl cyanide 4-(trifluoromethoxy)phenylhydrazone; Rote/AA: rotenone & antimycin A.

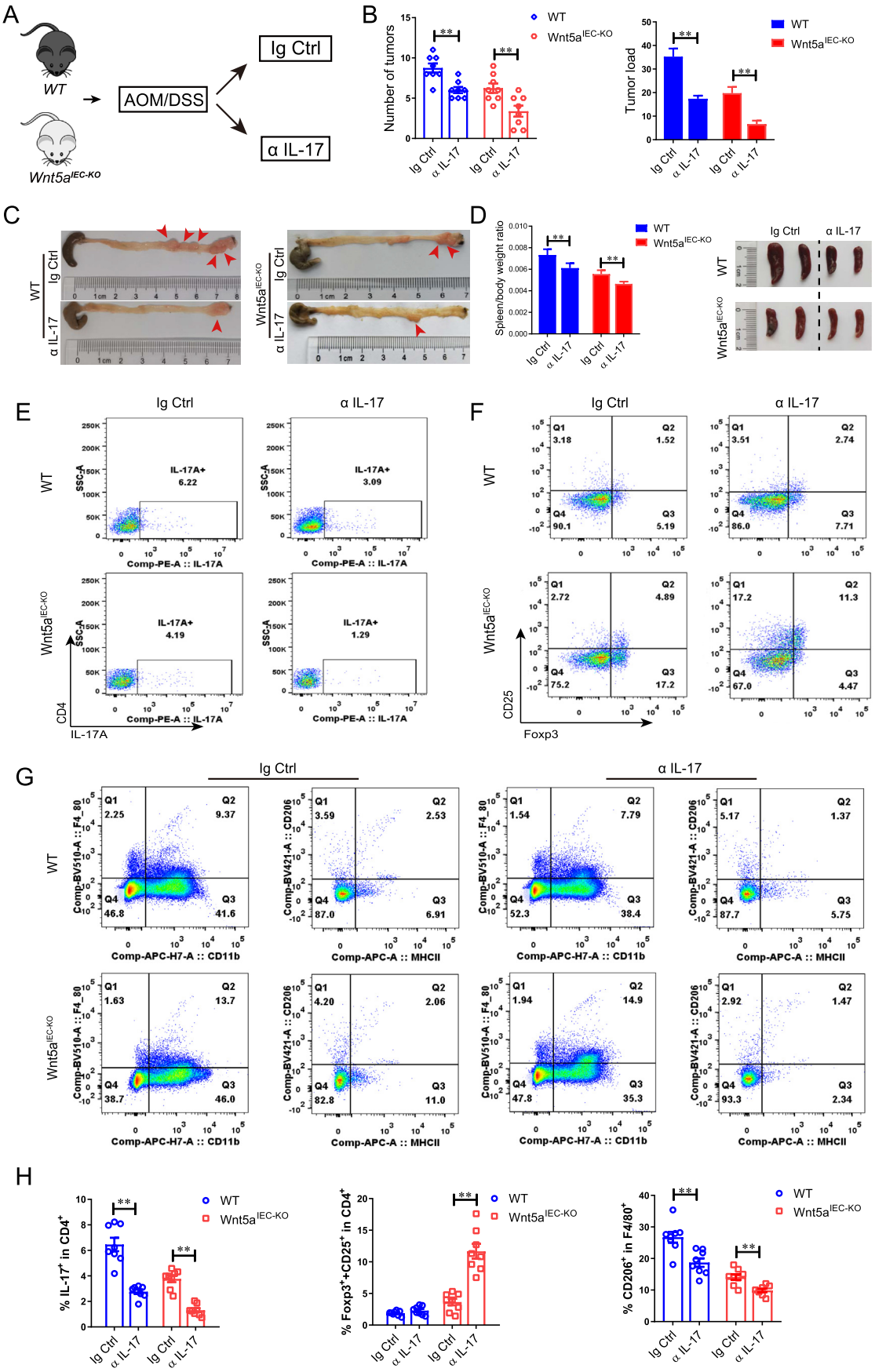

Fig. 6. T helper 17 (Th17) cell is mainly regulated by Wnt family member 5a (Wnt5a) during the process of tumor formation. (A) The procedures for interleukin-17A (IL-17A) injection in inducible knockout of *WNT5A* (*Wnt5a*$^{IEC\text{-}KO}$) mice induced by azoxymethane (AOM)/dextran sodium sulfate (DSS). IL-17A was injected one day after three cycles with

treatment (Fig. 6A). We observed that both anti-Th17 antibody and IgG treatment had no significant effect on body weight and hepatic and renal toxicity compared to their respective control group (data not shown). However, both tumor numbers and tumor loads were downregulated in mice after anti-IL17 treatment (Figs. 6B and 6C, and S6). Additionally, we found that the percentage of spleen weight index was decreased after anti-IL17 treatment compared to the untreated controls, indicating the lymphocyte activity could be decreased by Wnt5a-medicated Th17 cells (Fig. 6D). We then investigated the abundance of $CD4^+$, $CD25^+$, $Foxp3^+$, and $IL\text{-}17^+$ T cells within the total T cell population in the colon of $Wnt5a^{IEC\text{-}KO}$ mice and WT mice after AOM/DSS treatment. As expected, anti-IL17 treatment reduced the $IL17^+$ population in $CD4^+$ T cells and increased the $Foxp3^+$ population in $CD25^+/CD4^+$ T cells in $Wnt5a^{IEC\text{-}KO}$ mice after AOM/DSS treatment compared to WT mice after AOM/DSS treatment (Figs. 6E and F). Similar results were observed in M2 macrophage polarization (Figs. 6G and H).

3.7. YTE-17 suppresses intestinal tumorigenesis by the inhibition of β-catenin via Wnt5a/JNK signaling in TME

To activate the Wnt5a signal pathway, we administered the Wnt5a mimicking peptide Foxy5 (a 315 Wnt5a-derived hexapeptide, formyl-Met-Asp-Gly-Cys-Glu-Leu) via intraperitoneal injection to AOM/DSS-treated mice starting at week 10 (Fig. 7A). We found that Foxy5 dramatically increased tumor number (Figs. 7B, 7C, and S7), tumor load (Fig. 7D), degree of malignancy (Fig. 7E and Tables S2 [40] and S3), and ameliorated gross pathology and DAI score (Fig. 7F) in the AOM/DSS-treated mice compared to the control AOM/DSS-treated mice. Interestingly, this effect was attenuated when Foxy5 was combined with YTE-17, suggesting that YTE-17 resets macrophages, thereby improving the tumor immune microenvironment via the Wnt5a activation-dependent pathway.

Similarly, the protective effects of Wnt5a were associated with an improved β-catenin expression and proliferation of intestinal stem cells, as revealed by β-catenin labeling (Figs. 7G–I). Notably, Wnt5a also promoted the expression of β-catenin, a transcription factor known for its role in stem cells. This factor is a crucial component of canonical signaling, and is one of the most extensively studied non-β-catenin signaling members of the WNT family. Collectively, these data suggest that Wnt5a induces intestinal epithelial cells to promote macrophage-mediated Th17 cell glycolysis, thereby activating tumor stem cell differentiation and development through the β-catenin signaling pathway within the context of the TME.

4. Discussion

Garcinia yunnanensis, a local medicinal herb, has been traditionally exploited in traditional medicine for treating ulcers, wounds, suppuration, dysentery, and diarrhea [41]. However, the bioactive compounds of *Garcinia yunnanensis* (YTE-17), which consists of two structurally similar molecular compounds in a 1:1 ratio, and their potential anticancer effects have not been fully elucidated. In this study, we provide compelling evidence that YTE-17 exerts its antitumor effects primarily through the modulation of the immune system [6]. Our findings strongly support the immune-regulating function of YTE-17 in the context of anticancer activity (Fig. 8).

In recent years, extensive research has aimed to elaborate the intricate roles of immune cells in the transformation of inflammatory cancers [42,43]. A variety of studies have highlighted that the pivotal roles played by specific macrophage phenotype or subsets in tumor progression and their interactions with T cells. Consistent with previous reports [6], we found that YTE-17, with a no-toxicity dose, highly protected against tumorigenesis in CRC, as evidenced by its ability to regulate tumor burden, histological characteristics of tumors, and DAI scores in AOM/DSS mouse models of tumorigenesis. Subsequently, high-throughput raw signal analysis indicated that the expression of Wnt5a-related signaling pathway was significantly inhibited, suggesting a potential connection between YTE-17 and Wnt5a in inducing tumor stem cells. Consistent with other recent findings, the upregulation of Wnt5a, along with the activation of immune cells and inflammatory cytokines/chemokines, contribute to CRC carcinogenesis [44].

In this study, we used Villin-Cre-mediated deletion of Wnt5a in mice to elucidate the mechanism underlying the transformation of differentiated intestinal epithelial cells into colonic tumors. Our results are consistent with previous findings in mice, highlighting the critical role of Wnt5a in IECs to regulate the expression of immune and inflammatory modulators, particularly M2 macrophages, within the TME. Notably, the deletion of Wnt5a in IECs causes the imbalance between T-cell subsets and macrophages in the TME, which in turn protected against tumorigenesis by maintaining intestinal barrier integrity and regulating CSC progression. A recent study has unveiled that macrophages, as the predominant immune cells in the intestine, play diverse roles in regulating the function of T cells. Furthermore, TAMs can recruit Treg cells and promote CRC development in mice [45]. Moreover, M2 macrophages skewed the Treg/Th17 cell balance when co-cultured with T cells, likely due to the release of exosomes into the culture supernatant [46].

An important finding in this study is the role of M2 macrophages in regulating the differentiation of intestinal epithelial cells into colonic tumors through the modulation of the Treg/Th17 cell balance. Importantly, the addition of YTE-17 disrupts Wnt5a/JNK-induced polarization of TAM macrophage, thereby preventing Th17 phenotypic alterations. This suggests that YTE-17 mobilizes IECs to initiate macrophages and T-cell immune response for its antitumor effect. Furthermore, YTE-17's antitumor effect involves the suppression of TAM macrophage polarization, leading to increase glycolysis and the emergence of a Th17-like phenotype in the context of CRC. Our findings align with existing research and for the first time, clarify that YTE-17-induced IEC inhibits the TAM macrophages polarization and may further enhance glycolysis. This process leads to the development of an IL-17A-enriched microenvironment, $CD8^+$ T-cell exhaustion, and the promotion of colorectal carcinogenesis. Similar findings in AOM/DSS model showed that the depletion of the MondoA-TXNIP axis induced hyperglycolytic

AOM/DSS, and additional injections were performed every three days. (B, C) Inhibiting effect on tumorigenesis in $Wnt5a^{IEC\text{-}KO}$ mice with or without IL17 cells: tumor number (left) and tumor load (right) (B) and macroscopic view of the representative mouse intestinal shows several polypoid and discoid colonic tumors from mice in different groups (C). (D) Representative pictures of spleens from two groups. Spleen weight of mice was assessed on the right. (E–H) Flow cytometric analysis of IL-17-producing Th17 cells, regulatory T (Treg) cells in the $CD4^+$ lymphocyte population and M2 macrophage of lamina propria of wild-type (WT) mice and $Wnt5a^{IEC\text{-}KO}$ mice with or without Th17 cells ($n = 8$ each): positive expressions of CD4 and IL-17A (E), CD25 and forkhead box protein 3 (Foxp3) (F), and CD206 and F4/80 (G), as well as summary graph proportion for each group (H). Data are presented as a representative FACS plot (E–G) and summary graph (H) (each circle represents a mouse). The data are presented as the mean ± standard deviation (SD) ($n = 5$), with Welch's correction, one-tailed *t*-test. $^{**}P < 0.01$ vs. WT mice treatment with AOM/DSS administration. IEC: intestinal epithelial cells; Foxp3: forkhead box protein 3.

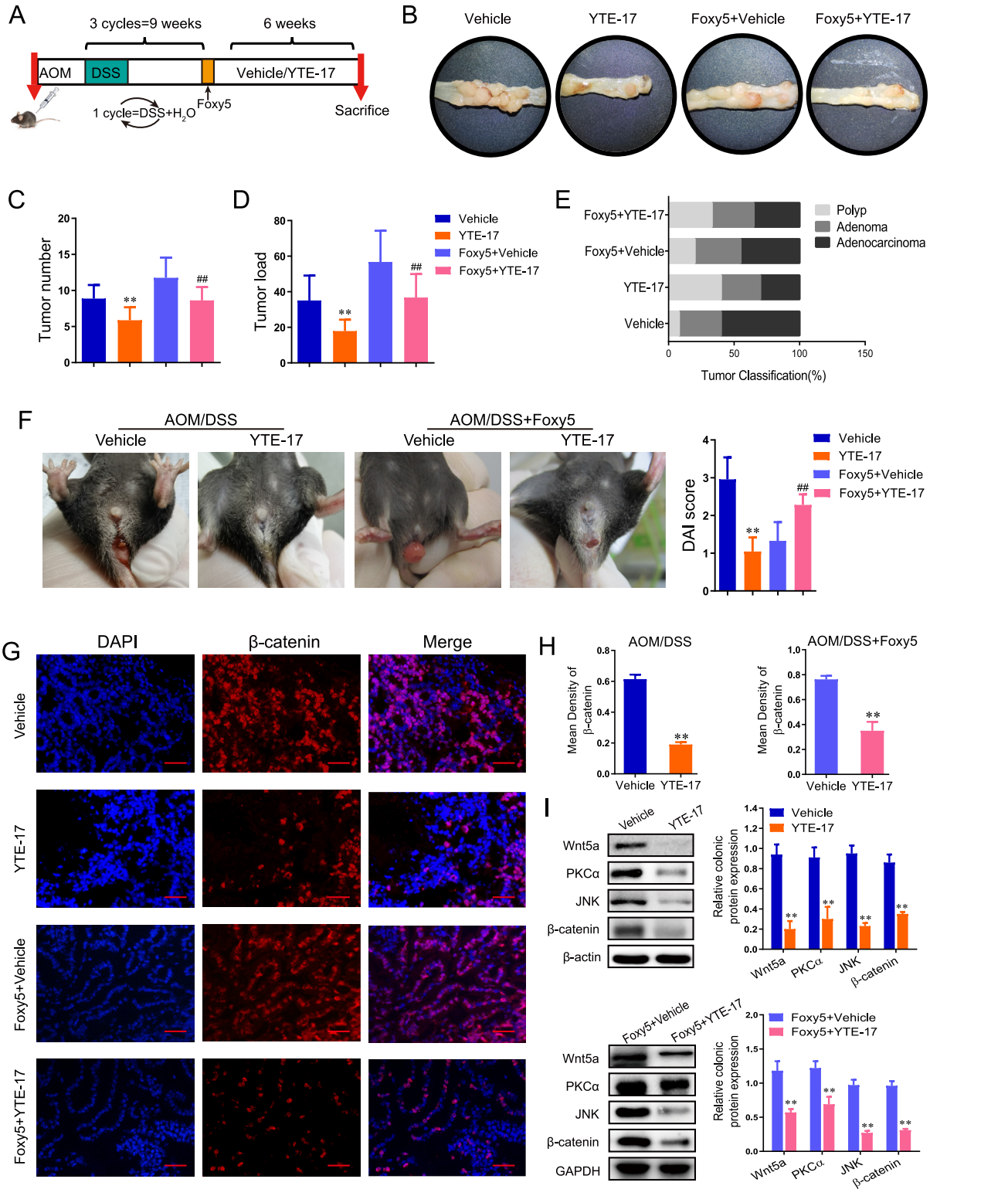

Fig. 7. Effect of *Garcinia yunnanensis* (YTE-17) on Wnt family member 5a (Wnt5a) medicated catenin pathway in azoxymethane (AOM)/dextran sodium sulfate (DSS) mice with Foxy5. (A) Experimental design indicating the timing of the intragastric administration and organization of groups. Mice were treatmented with AOM/DSS for nine weeks as described in the Supplementary data and injected with Foxy5 (12.5 mg/kg, i.p.) at the first day of Week 10 (matching with Fig. 1I), then intragastric administration with YTE-17 for nine weeks. (B–D) Effect of YTE-17 on tumorigenesis in AOM/DSS mice with Foxy5. Macroscopic view of the representative mouse intestinal (B), tumor number (C), and tumor load (D). (E) Histology evaluation of colon tumors: quantitatively represented as polyp, adenoma, and adenocarcinoma. (F) Rectal bleeding and/or rectocele disease activity index, disease activity index (DAI), body weights, stool, and body posture were monitored daily to assess DAI. (G) Immunofluorescence micrographs of 4′,6-diamidino-2-phenylindole (DAPI) (blue) and β-catenin (red) expression. (H) Relative fluorescence density analysis of β-catenin in the colons of AOM/DSS mice with or without YTE-17 (left), and in the colons of AOM/DSS mice after the addition of Foxy5, mice were treatment with of without YTE-17(right). (I) Western blots showing expression levels of β-catenin, GSK-3β, TCF4, and LEF1 in the colons of AOM/DSS mice with or without YTE-17 (up) and Foxy5 addition with/without YTE-17 (down). Data are presented as the means ± standard deviation (SD) of eight animals per experimental group with Welch's correction, two-tailed *t*-test. $^{**}P < 0.01$, vehicle vs. YTE-17; $^{\#\#}P < 0.01$, Foxy5 + vehicle vs. Foxy5 + YTE-17. PKCα: protein kinase C-alpha; JNK: c-Jun N-terminal kinase; GAPDH: glyceraldehyde-3-phosphate dehydrogenase.

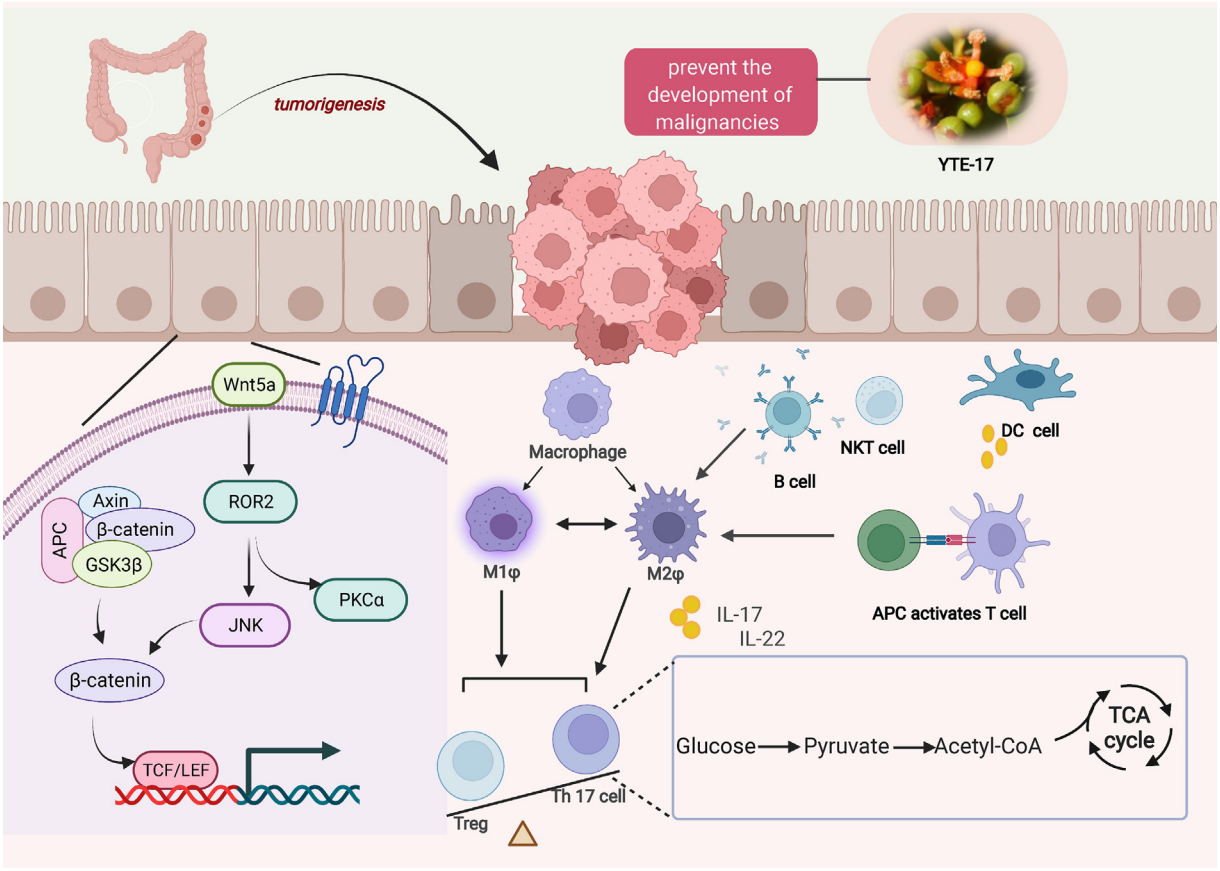

Fig. 8. Schematic diagram of the mechanism of *Garcinia yunnanensis* (YTE-17) in tumor microenvironment (TME) during colorectal carcinogenesis. YTE-17 reverse the polarization of M2 macrophage in tumor-associated macrophage (TAM) type and inhibition enhanced glycolysis of T helper 17 (Th17) cells, leading to recover the disorder of regulatory T (Treg)/Th17 cell balance and prevent colorectal carcinogenesis. Wnt5a: Wnt family member 5a; ROR2: receptor tyrosine kinase-like orphan receptor 2; PKCα: protein kinase C-alpha; JNK: c-Jun N-terminal kinase; APC: adenomatous polyposis coli; TCF: transcription factor T cell factor; LEF: lymphoid enhance factor; NKT: natural killer T cell; DC: dendritic cells; IL: interleukin; TCA: tricarboxylic acid cycle.

Th17-like Treg cells, which facilitated Th17 cell inflammation, promoted $CD8^+$ T-cell exhaustion, and drove colorectal carcinogenesis [39]. Interestingly, in our study, the glycolysis of Th17 cell triggered by macrophage polarization was found to be a driver of epithelial cell carcinogenesis.

Another crucial aspect of our research is the elucidation of the non-canonical WNT/JNK signaling in β-catenin activity promoting the malignant transfromation of IECs into CRCs. A recent study of mutational landscape of human CAC tissues revealed that mutations in non-canonical WNT associated pathways, such as the Rho and Rac GTPase network components, are observed in about 50% of CAC samples, but rarely observed in sporadic CRC samples [47]. This underscores the importance of non-canonical WNT pathways in CAC development. While it is well-established that the activation of the canonical Wnt/β-catenin pathway is an initiating event in the majority of human CRCs and one of the key regulators of CRC pathogenesis [48], most studies have also confirmed that Wnt5a is positively correlated the development of CRC in a positive proportion [49,50]. This study shed light on the possible mechanisms between non-canonical Wnt5a/JNK signaling and well-known canonical β-catenin oncogenic pathway *in vivo*. Specifically, Wnt5a/JNK signaling activity in IECs promotes the development of cancer stem cells with β-catenin activity in the presence of macrophages and T cells within TME. These findings align with previous reports indicating that Th17 cell differentiation involves the transcription of TCF/LEF as downstream of β-catenin signaling, contributing to the carcinogenic processes in the colon and intestine [20].

5. Conclusions

In summary, our findings revealed the significant role of YTE-17 in delaying the progression of CRC carcinogenesis via down-regulating biological functions of Wnt5a. which subsequently promotes the development of intestinal epithelial cells as tumor stem cells. The evidence supporting these effects includes the observed changes in tumor load in Wnt5a-deficient mice treated with AOM/DSS and the formation of CSC-like spheres. Specifically, we have demonstrated that the cancer cell growth can be influenced by the macrophage polarization via Th17 cell induction. This is substantiated by our findings that YTE-17 treated IECs inhibited M2 macrophage polarization by suppressing Th17 cell glycolysis. Furthermore, our study reveals a critical link between non-canonical Wnt stimulation and β-catenin activation, facilitated by M2 macrophage polarization and Th17 cell glycolysis. This enhances CSC activation and contributes to CRC development.

This discovery deepens our understand of YTE-17's anticancer effects and its capacity to remodel the immune microenvironment, leading to regulation of immunity and delay of carcinogenesis.

Future studies will address functional significance of the loss of the Wnt5a in the spontaneous intestinal TME. This research may ultimately pave the way for the use of YTE-17 in immunotherapy strategies for CRC.

CRediT author statement

Hua Sui, **Wanli Deng**, and **Qiong Chai:** Project administration, Methodology, Validation, Investigation, Writing - Original draft preparation; **Bing Han**, **Yuli Zhang**, **Zhenzhen Wei**, and **Zan Li:** Data curation, Software; **Ting Wang**, **Jiling Feng**, and **Man Yuan:** Visualization, Investigation; **Qingfeng Tang** and **Hongxi Xu:** Writing - Reviewing and Editing, Project administration.

Declaration of competing interest

The authors declare that there are no conflicts of interest.

Acknowledgments

This research was supported by "Jiaotong University Star" Program, China (Grant No.: YG2022QN082), the National Natural Science Foundation of China (Grant No.: 82204887), the Science Foundation for Shanghai Committee of Science Project, China (Grant Nos.: 21S21901400 and 23S21901200), and the Natural Science Research Foundation of Jiading District, China (Grant No.: JDKW-2021-0023).

Appendix A. Supplementary data

Supplementary data to this article can be found online at https://doi.org/10.1016/j.jpha.2023.11.008.

References

[1] L. Zhang, Z. Li, K.M. Skrzypczynska, et al., Single-cell analyses inform mechanisms of myeloid-targeted therapies in colon cancer, Cell 181 (2020) 442–459.e29.
[2] X. Ma, Z. Meng, L. Jin, et al., CAMK2γ in intestinal epithelial cells modulates colitis-associated colorectal carcinogenesis via enhancing STAT3 activation, Oncogene 36 (2017) 4060–4071.
[3] O. Dmitrieva-Posocco, A.C. Wong, P. Lundgren, et al., β-Hydroxybutyrate suppresses colorectal cancer, Nature 605 (2022) 160–165.
[4] Q. Li, W. Hu, W.-X. Liu, et al., *Streptococcus thermophilus* inhibits colorectal tumorigenesis through secreting β-galactosidase, Gastroenterology 160 (2021) 1179–1193.e14.
[5] A. Malik, D. Sharma, R.K.S. Malireddi, et al., SYK-CARD9 signaling axis promotes gut fungi-mediated inflammasome activation to restrict colitis and colon cancer, Immunity 49 (2018) 515–530.e5.
[6] H. Sui, H. Tan, J. Fu, et al., The active fraction of *Garcinia yunnanensis* suppresses the progression of colorectal carcinoma by interfering with tumor-associated macrophage-associated M2 macrophage polarization *in vivo* and *in vitro*, FASEB J. 34 (2020) 7387–7403.
[7] H. Miyoshi, R. Ajima, C.T. Luo, et al., Wnt5a potentiates TGF-β signaling to promote colonic crypt regeneration after tissue injury, Science 338 (2012) 108–113.
[8] S. Rogers, S. Scholpp, Vertebrate Wnt5a - At the crossroads of cellular signalling, Semin. Cell Dev. Biol. 125 (2022) 3–10.
[9] K. Wang, F. Ma, S. Arai, et al., WNT5a signaling through ROR2 activates the Hippo pathway to suppress YAP1 activity and tumor growth, Cancer Res. 83 (2023) 1016–1030.
[10] D. Hasegawa, N. Wada, S. Yoshida, et al., Wnt5a suppresses osteoblastic differentiation of human periodontal ligament stem cell-like cells via Ror2/JNK signaling, J. Cell. Physiol. 233 (2018) 1752–1762.
[11] D. Bayik, J.D. Lathia, Cancer stem cell-immune cell crosstalk in tumour progression, Nat. Rev. Cancer 21 (2021) 526–536.
[12] L. Fan, C. Xu, Q. Ge, et al., *A. muciniphila* suppresses colorectal tumorigenesis by inducing TLR2/NLRP3-mediated M1-like TAMs, Cancer Immunol. Res. 9 (2021) 1111–1124.
[13] C.M. Schurch, S.S. Bhate, G.L. Barlow, et al., Coordinated cellular neighborhoods orchestrate antitumoral immunity at the colorectal cancer invasive front, Cell 182 (2020) 1341–1359.e19.
[14] H. Sui, L. Zhang, K. Gu, et al., YYFZBJS ameliorates colorectal cancer progression in $Apc^{Min/+}$ mice by remodeling gut microbiota and inhibiting regulatory T-cell generation, Cell Commun. Signal. 18 (2020), 113.
[15] S. Hang, D. Paik, L. Yao, et al., Bile acid metabolites control T_H17 and T_{reg} cell differentiation, Nature 576 (2019) 143–148.
[16] A. Wagner, C. Wang, J. Fessler, et al., Metabolic modeling of single Th17 cells reveals regulators of autoimmunity, Cell 184 (2021) 4168–4185.e21.
[17] Y.S. Zhang, D.E. Xin, Z. Wang, et al., STAT4 activation by leukemia inhibitory factor confers a therapeutic effect on intestinal inflammation, EMBO J. 38 (2019), e99595.
[18] F. Zhu, H. Li, Y. Liu, et al., miR-155 antagomir protect against DSS-induced colitis in mice through regulating Th17/Treg cell balance by Jarid2/Wnt/β-catenin, Biomed. Pharmacother. 126 (2020), 109909.
[19] A. Osman, B. Yan, Y. Li, et al., TCF-1 controls T_{reg} cell functions that regulate inflammation, $CD8^+$ T cell cytotoxicity and severity of colon cancer, Nat. Immunol. 22 (2021) 1152–1162.
[20] R. Kinoshita-Daitoku, K. Kiga, M. Miyakoshi, et al., A bacterial small RNA regulates the adaptation of *Helicobacter pylori* to the host environment, Nat. Commun. 12 (2021), 2085.
[21] N. Chai, Y. Xiong, Y. Zhang, et al., YYFZBJS inhibits colorectal tumorigenesis by remodeling gut microbiota and influence on M2 macrophage polarization *in vivo* and *in vitro*, Am. J. Cancer Res. 11 (2021) 5338–5357.
[22] H. Nienhuser, W. Kim, E. Malagola, et al., Mist1+ gastric isthmus stem cells are regulated by Wnt5a and expand in response to injury and inflammation in mice, Gut 70 (2021) 654–665.
[23] M. Asem, A.M. Young, C. Oyama, et al., Host Wnt5a potentiates microenvironmental regulation of ovarian cancer metastasis, Cancer Res. 80 (2020) 1156–1170.
[24] H. Li, X. Meng, L. Zhang, et al., Oblongifolin C and guttiferone K extracted from Garcinia yunnanensis fruit synergistically induce apoptosis in human colorectal cancer cells *in vitro*, Acta Pharmacol. Sin. 38 (2017) 252–263.
[25] D.J. Flanagan, N. Pentinmikko, K. Luopajarvi, et al., NOTUM from Apc-mutant cells biases clonal competition to initiate cancer, Nature 594 (2021) 430–435.
[26] G. Singovski, C. Bernal, M. Kuciak, et al., *In vivo* epigenetic reprogramming of primary human colon cancer cells enhances metastases, J. Mol. Cell Biol. 8 (2016) 157–173.
[27] Z. Li, L. Mao, B. Yu, et al., GB7 acetate, a *galbulimima* alkaloid from *Galbulimima belgraveana*, possesses anticancer effects in colorectal cancer cells, J. Pharm. Anal. 12 (2022) 339–349.
[28] D.T. Miyamoto, Y. Zheng, B.S. Wittner, et al., RNA-Seq of single prostate CTCs implicates noncanonical Wnt signaling in antiandrogen resistance, Science 349 (2015) 1351–1356.
[29] G. Fuertes, B. Del Valle-Perez, J. Pastor, et al., Noncanonical Wnt signaling promotes colon tumor growth, chemoresistance and tumor fibroblast activation, EMBO Rep. 24 (2023), e54895.
[30] J. Osman, K. Bellamkonda, Q. Liu, et al., The WNT5A agonist Foxy5 reduces the number of colonic cancer stem cells in a xenograft mouse model of human colonic cancer, Anticancer Res. 39 (2019) 1719–1728.
[31] X. Wei, J. Gong, J. Ma, et al., Targeting the Dvl-1/β-arrestin2/JNK3 interaction disrupts Wnt5a-JNK3 signaling and protects hippocampal CA1 neurons during cerebral ischemia reperfusion, Neuropharmacology 135 (2018) 11–21.
[32] J. Zhang, C. Wang, Z. Guo, et al., miR-223 improves intestinal inflammation through inhibiting the IL-6/STAT3 signaling pathway in dextran sodium sulfate-induced experimental colitis, Immun. Inflamm. Dis. 9 (2021) 319–327.
[33] T.-W. Kim, J.-S. Shin, K.-S. Chung, et al., Anti-inflammatory mechanisms of koreanaside A, a lignan isolated from the flower of Forsythia koreana, against LPS-induced macrophage activation and DSS-induced colitis mice: The crucial role of AP-1, NF-κB, and JAK/STAT signaling, Cells 8 (2019), 1163.
[34] L. Dong, J. Xie, Y. Wang, et al., Mannose ameliorates experimental colitis by protecting intestinal barrier integrity, Nat. Commun. 13 (2022), 4804.
[35] M. Lleal, G. Sarrabayrouse, J. Willamil, et al., A single faecal microbiota transplantation modulates the microbiome and improves clinical manifestations in a rat model of colitis, EBioMedicine 48 (2019) 630–641.
[36] H. Tilg, T.E. Adolph, R.R. Gerner, et al., The intestinal microbiota in colorectal cancer, Cancer Cell 33 (2018) 954–964.
[37] J. Roelands, M. van der Ploeg, M.E. Ijsselsteijn, et al., Transcriptomic and immunophenotypic profiling reveals molecular and immunological hallmarks of colorectal cancer tumourigenesis, Gut 72 (2023) 1326–1339.
[38] E. Loeuillard, J. Yang, E. Buckarma, et al., Targeting tumor-associated macrophages and granulocytic myeloid-derived suppressor cells augments PD-1 blockade in cholangiocarcinoma, J. Clin. Invest. 130 (2020) 5380–5396.
[39] Y. Lu, Y. Li, Q. Liu, et al., MondoA-thioredoxin-interacting protein axis maintains regulatory T-cell identity and function in colorectal cancer microenvironment, Gastroenterology 161 (2021) 575–591.e16.
[40] T. Poutahidis, V.P. Rao, W. Olipitz, et al., $CD4^+$ lymphocytes modulate prostate cancer progression in mice, Int. J. Cancer 125 (2009) 868–878.
[41] Y.L. Phang, C. Zheng, H. Xu, Structural diversity and biological activities of caged Garcinia xanthones: Recent updates, Acta Mater. Med. 1 (2022) 72–95.
[42] Y. Zhang, L. Huo, Z. Wei, et al., Hotspots and frontiers in inflammatory tumor microenvironment research: A scientometric and visualization analysis, Front. Pharmacol. 13 (2022), 862585.

[43] Y. Zhang, N. Chai, Z. Wei, et al., YYFZBJS inhibits colorectal tumorigenesis by enhancing Tregs-induced immunosuppression through HIF-1α mediated hypoxia *in vivo* and *in vitro*, Phytomedicine 98 (2022), 153917.
[44] X. Bai, R. Fu, Y. Liu, et al., Ginsenoside Rk3 modulates gut microbiota and regulates immune response of group 3 innate lymphoid cells to against colorectal tumorigenesis, J. Pharm. Anal. 14 (2024) 259–275.
[45] B. Xin, M. Yang, P. Wu, et al., Enhancing the therapeutic efficacy of programmed death ligand 1 antibody for metastasized liver cancer by overcoming hepatic immunotolerance in mice, Hepatology 76 (2022) 630–645.
[46] J. Zhou, X. Li, X. Wu, et al., Exosomes released from tumor-associated macrophages transfer miRNAs that induce a Treg/Th17 cell imbalance in epithelial ovarian cancer, Cancer Immunol. Res. 6 (2018) 1578–1592.
[47] A.I. Robles, G. Traverso, M. Zhang, et al., Whole-exome sequencing analyses of inflammatory bowel disease-associated colorectal cancers, Gastroenterology 150 (2016) 931–943.
[48] J. Quandt, S. Arnovitz, L. Haghi, et al., Wnt-β-catenin activation epigenetically reprograms T_{reg} cells in inflammatory bowel disease and dysplastic progression, Nat. Immunol. 22 (2021) 471–484.
[49] M. Pashirzad, T. Sathyapalan, A. Sahebkar, Clinical importance of Wnt5a in the pathogenesis of colorectal cancer, J. Oncol. 2021 (2021), 3136508.
[50] Q. Liu, C. Yang, S. Wang, et al., Wnt5a-induced M2 polarization of tumor-associated macrophages via IL-10 promotes colorectal cancer progression, Cell Commun. Signal. 18 (2020), 51.